DEVELPOMENT OF CALCULATION APPROACH FOR THE DETERMINATION OF CENTRAL AXIS DEPTH DOSES IN WATER FOR COBALT 60 BEAM.

THIS THESIS IS SUBMITTED TO THE

DEPARTMENT OF MEDICAL PHYSICS

SCHOOL OF NUCLEAR AND ALLIED SCIENCES

UNIVERSITY OF GHANA, LEGON

BY

ADDO, DORCAS OFORIWAAH

(10598778)

IN PARTIAL FULFILLMENT OF THE REQUIREMENT FOR THE AWARD OF **MASTER OF PHILOSOPHY DEGREE IN MEDICAL PHYSICS DEGREE.**

JULY 2018

DECLARATION

"This thesis is a result of a research work undertaken by Dorcas Oforiwaah Addo in the department of medical physics, School of Nuclear and Allied Sciences, University of Ghana, under the supervision of Professor Cyril Schandorf, Mr. Samuel Nii Adu Tagoe and Dr. Francis Hasford." I hereby affirm that except for references which have been cited, this work is a product of my own research and it has not been presented in part or whole for any other degree in this University or elsewhere.

Sign…… Date……

Dorcas Oforiwaah Addo

(Student)

Sign…… Date….....

Prof. Cyril Schandorf

(Principal Supervisor)

Sign…… Date……

Mr. Samuel N.A. Tagoe

(Co-supervisor)

Sign…… Date……..

Dr. Francis Hasford

(Co-supervisor)

ABSTRACT

Radiotherapy is a complicated procedure with several steps, and these procedures have a great influence on the treatment outcome. Exact determination of dosimetric functions that are used to calculate dose within a patient undergoing external beam radiotherapy to realize the intent of treatment is very crucial for any radiotherapy treatment technique. One of the dosimetric functions, which is of great importance, is central axis percentage depth dose, which are usually measured with automated systems. The aim of the current study was to develop and propose a semi-empirical formula that can be used to determine central axis percentage depth doses through manual calculations. This could also be used as a quality assurance tool to check uncertainties associated with measured central axis depth doses.

Linear attenuation coefficients of water were measured for water with beams from a Theratron Equinox 100 cobalt 60 teletherapy unit using field sizes ranging from 4 cm x4 cm to 30 cm x30 cm, to determine the effective linear attenuation of water within a formula obtained from literature to express the primary component of percentage depth dose (PDD). The linear attenuation coefficient measurements were done in air with a 0.125 cc Semiflex ionization chamber with its build-up cap on. With the expression for the primary component of the percentage depth doses (PDD) and measured PDD data obtained during commissioning of the telecobalt machine, a semi-empirical formula was developed and proposed for the determination of PDD, which considered both the primary, and the scatter components of the PDD.

The PDDs calculated with the proposed semi-empirical formula compared very well with their measured counterpart with percentage differences between measured and calculated PDDs ranging from 0.10% to 2.01% (mean of 1.24±0.88%), which is within the 2%

acceptable limit for central axis parameter constancy (PDD, TAR) as recommended in the report of the TG-40

The use of the proposed formula for calculating PDD is recommended for clinical application, but one needs to be circumspective in the use of the formula as some few PDDs (2%) calculated with the formula compared to their measured counterparts were found to have discrepancies beyond the tolerance of 2% recommended for the determination of central axis depth doses.

ACKNOWLEDGEMENTS

I am very grateful to my supervisors, Professor Cyril Schandorf, Mr. Samuel Nii Adu Tagoe and Dr. Francis Hasford. for their patience, intellectual guidance and encouragement; may the favor of God never cease on him.

I also recognize and thank Dr. Awuah of the Ghana Atomic Energy Commission Medicine: RAMSRI for his guidance and all the lecturers in the department of physics for their diverse contribution to the completion of this work.

Finally, I am very grateful to Madam Beatrice Nyarko for her undying support and encouragement. I say thank you all and may almighty God richly bless you all.

DEDICATION

This research work is dedicated to my mother, Madam Beatrice Nyarko.

TABLE OF CONTENTS

LIST OF FIGURES

LIST OF TABLES

LIST OF ABBREVIATIONS AND SYMBOLS

AAPM	American association of physicists in medicine
KERMA	Kinetic energy released in matter
TERMA	Total energy released in matter
TG43	Task group 43
TPS	Treatment planning system
2D	Two dimension
3D	Three dimension
Co-60	Cobalt 60 Source
KBTH	Korle -Bu Teaching Hospital
NCRNM	National Center for Radiotherapy and Nuclear Medicine
QA	Quality Assurance
QC	Quality control
TLD	Thermoluminiscent dosimeter
CT	Computerized tomography
MRI	Magnetic Resonance Imaging
D_0	Reference depth
D_{max}	Dose at maximum depth
IAEA	International Atomic Energy Agency
ICRU	International Commission On Radiation Units and Measurements
OF	Output Factor
PDD	Percentage Depth Dose
PDD_P	Primary component of Percentage Depth Dose

Ks	Scattered component of Percentage Depth Dose
PSF	Peak Scatter Factor
S_C	Collimator Scatter Factor
S_P	Phantom Scatter Factor
S_{Cp}	Total Scatter Factor
SSD	Source to Surface Distance
SAD	Source to Axis Distance
CA	Central Axis
D_P	Primary Dose
TMR	Tissue Maximum Ratio
TAR	Tissue Air Ratio
PMMA	Polymethyl methacrylate
TF	Transmission Factor
MC	Monte Carlo
LAC / μ	Linear Attenuation Coefficient
μeff	Effective Linear attenuation coefficient
A	Field Size
D	Depth
hv	Photon Energy
Gy	Gray
cm	Centimeter
M	Mass
Kg	Kilogram

MV	Megavoltage
MeV	Mega electron Voltage
D	Absorbed Dose
Z	Atomic number
ϒ	Gamma ray

APPENDICE

CHAPTER ONE

INTRODUCTION

1.1 BACKGROUND

Radiotherapy is a complicated procedure with several steps, and these procedures have a great influence on the treatment quality. Exact determination of dosimetric functions to aid in the estimation of dose distribution with a patient undergoing external beam radiotherapy (EBRT) is paramount to any radiotherapy technique (Memon, et al., 2014).

For attaining a uniform dose distribution within the target volume (tumour plus margin to account for variations in tumour localization uncertainties) and the smallest conceivable dose to the healthy neighboring tissues close to the target volume, external photon beam radiotherapy is generally performed using multiple radiation beam (Memon, et al., 2014).

The advance and development in radiation therapy offers significant improvement in clinical accuracy and precision in the delivery of dose in treatment compared with earlier calculation methods (Chaikh et al., 2016).

These advancement and development have enhanced dose determination and treatment delivery in EBRT. Effective optimization approaches are needed to deliver the exact prescribed dose to the tumour to achieve high tumour control probability (TCP) and low normal tissue complication probability (NTCP) for organs at risk (OARs). International Commission on Radiation Units and Measurements (ICRU) has proposed an overall dose accuracy within ± 5% (Chaikh et al., 2016).

In preventing excessive and unjustifiable exposure to ionizing radiation, it is obligatory to define the dose distribution for particular body organs and tissues referring to IAEA protocols (Memon, et. al., 2014).

Dose distribution within a patient is the most recognizable parameter that links treatment parameters of any radiotherapy treatment technique to treatment outcome. It is therefore imperative to know with great accuracy the dose that will be deposited at any point within the patient. The dose distributions within a patient are calculated based on certain beam data that are measured in a water phantom. Dosimetric functions such as percentage depth dose (PDD), relative output factor and dose profiles are used to link the beam data measured in the water phantom to the dose distribution within the patient (Xhafa1et al., 2014). Taking into consideration the uncertainties associated with the measurements of the required beam data, especially PDD, it will be appropriate to develop a semi-empirical calculation approach to help in checking accuracy of the measured beam data. This will enhance the accuracy of dose distribution calculations and aid in achieving the recommended uncertainty tolerance of less than 3% accuracy (Chaikh et al., 2016).

PDD is a crucial dosimetric function, which gives an idea of how the dose varies with depth within the patient. In clinical practice, other dosimetric functions like tissue phantom ratio (TPR) and tissue maximum ratio (TMR), which are also used to indicate variation of dose with depth for isocentric treatment technique, are usually derived from measured PDD data (Xhafa1et al., 2014).

PDD can also be used as a beam quality specifier for megavoltage beams. PDD is the only dosimetric function that is defined for all beam energies used in radiotherapy. PDD data are also needed by treatment planning systems for patient dose modeling. PDD data are

usually acquired with motorized water tank systems, which comprises of a computer control detector holder system placed in a full scatter water tank and a telescopic lifting carriage for the tank.

To obtain the PDD, absorbed dose measurements are generally measured on the beam central axis for various depths and then normalized to that of a reference depth (usually the depth of maximum dose) for a specific beam energy, field size and source to surface distance (SSD) (Xhafa1et al., 2014). Absorbed dose measured on the beam central axis for a particular depth is termed the central axis depth dose. PDD is therefore dependent on beam energy, field size and SSD. Field size is the area covered for treatment, which in clinical settings need to be determined dosimetrically. PDD for constant field size, depth and SSD increases with increasing beam energy, due to increase in the penetrability of the beam resulting in more dose being deposited at any depth within a medium. Increase in field size increase the PDD in a medium due to more scattered radiations contribution to dose at any point within a medium. On the other hand, PDD decreases with increasing depth and this is due to beam attenuation. PDD increases with increasing SSD due to the divergence nature of beams coming from teletherapy machines, which causes scattered radiation contribution to dose at any point to overshadow the effect of the inverse square law.

1.2 STATEMENT OF PROBLEM

In clinical settings, automated systems are used in the acquisition of PDD data due to convenience and the difficulty in stabilizing environmental conditions prevailing at the area of measurements. These automations may be prone to uncertainties, which would be

difficult to detect. Developing a manual calculation approach for the determination of PDD can be used to check against the PDD measured with the automation systems.

1.3 OBJECTIVES OF THE RESEARCH STUDY

The principal objective of this research was to develop and propose a calculation approach for the determination of PDD (with respect to some dosimetric functions) that would aid in assessing dose distribution and clinically serve as a manual quality control check for quick verification of measured PDD data.

Specific objective of research includes:

- To obtain the effective linear attenuation coefficient of water for the proposed expression for the primary component of PDD for cobalt 60 beam.
- To determine the scatter component of PDD for cobalt 60 beam based on the measured PDD data obtained during commissioning.
- To develop a semi-empirical formula for calculating the determined scatter component of the PDD in terms of field size and treatment depth (depth within water).
- To propose a semi-empirical formula for the determination of PDD to include both the primary and scatter component.
- To make appropriate recommendation(s) from the study.

1.4 RELEVANCE AND JUSTIFICATION

This semi-empirical formula would serve as a manual check for Equinox 100 teletherapy machine and clinically serve as a quality control check to minimize error.

1.5 SCOPE AND DELIMITATION

Linear attenuation coefficient (LAC) would be measured for water with different field sizes in air and PDD data acquired during the commissioning of the Equinox 100 teletherapy machine at the National Centre for Radiotherapy and Nuclear Medicine (NCRNM), Korle-Bu teaching hospital will be acquired for the study. The measured PDD data and proposed formula for the determination of the primary component of PDD from literature would be used to develop a semi-empirical formula for the determination of the PDD for the telecobalt machine.

Since PDD within the build-up region is difficult to predict, depths greater than the depth of maximum dose (d_{max}) would be considered in developing the semi- empirical formula.

Field size smaller than 3 cm x 3 cm would not be included in the measurement of LAC due to the size of the ionization chamber (semiflex) used for the measurement.

1.6 ORGANIZATION OF THESIS

The thesis is organised as follows:

Chapter one is the introduction which provides the background of the studies, problem of statement of the research, objectives, relevance and justification and scope and delimitation.

Chapter two contains a detailed review of the literature relevant to the research study, Chapter three gives a description of the materials and methods used to carry out the research work,

Chapter four gives an account of the results obtained and discussion of the findings in relation to peer reviewed published works. Chapter five provides the conclusions of the research work and recommendations addressed to relevant stakeholders.

CHAPTER TWO

LITERATURE REVIEW

2.0 RADIOTHERAPY

Radiation therapy (also called radiotherapy) is a cancer treatment that uses high doses of radiation to kill cancer cells and shrink tumors. There are two types of radiotherapy: external beam radiotherapy, where the source of radiation is placed outside the patient and radiation beams are delivered to a specific target volume; this method is referred as the three-Dimensional Conformal Radiotherapy (3DCRT). The target or tumor volume (the disease) is modelled and the radiations are focused to this volume. Therefore, the dose of radiations hitting the healthy cells of the anatomically adjacent organs, which are not affected by the illness, can be reduced. The second type of radiotherapy is brachytherapy. Brachytherapy is done by placing a sealed radioactive source in close proximity to the target or in the target volume. The radioactive material comes in different in shape and size (wires, capsules, spheres). In brachytherapy, the source can either be permanently or temporarily implanted.

According to Ahnesjo and Aspradakis, (1999), in early radiotherapy, the term 'dose' was used in a pharmacological sense to measure the quantity of radiation to be delivered instead of the physical effect on the matter being exposed to radiation. The definition of absorbed dose according to the ICRU report number 24 is strictly the average energy contributed per unit mass by ionizing radiation, which means dose dissociates from the used radiation and distribution. Thus, dose absorbed serves as a significant physical quantity, which is of importance for associating radiation treatment to its effects (ICRU 1998).

Dose can be measured in absolute terms using Calorimeters and ionization chambers but are inappropriate in terms of *'in vivo* dosimetry'. In addition, dose delivered in patients can be determined by placing Thermoluminescence detectors and diodes placed in contact with the surface of the patient body at the point of beam entrance otherwise, sometimes inside the cavums (cavities) of the patient, but this is inappropriate for gaining a plan of the dose. Therefore, to quantify the distributions of dose in patients, it is necessary to base it on calculation ideals and examples for planning treatment and in delivered treatment follow-up.

Generally, dosimetric functions are evaluated in a homogeneous water phantom for dose determination in radiotherapy. Unjustifiable ionizing radiation exposure can be avoided by defining a radiation dose to particular organs and tissues of the body in accordance to the protocols of the IAEA, 2000 (Memon et al., 2014). According to the reports of the ICRU, the present reasonable amount for the exact conditions for a recommended dose to the target volume is 2% to 3%. Accuracy in calculating dose is necessary in the patient's radiotherapeutic treatment, thus the error of total dose delivery to patients must not go beyond 5%, as recommended by the ICRU, 1993 and Nordic Association of Clinical Physicists (NACO) (Memon et al., 2014). In radiation oncology, more importance is attached to delivering precise radiation dose to a prescribed target region, using the smallest amount of dose to normal tissues.

The only option that was available to medical physicists included formulation of empirical methods for dose calculation as soon as photon beams with high-energy were made available for clinical use since 1950s. These methods usually limited the treatments to beam set-ups which may well be evaluated (Ahnesjö & Ahnesj, 2014).

Methods that are empirical are restricted in the degree of accuracy, and thus incapable of modeling generalized beam set-ups. Possibility of analytical methods working will occur for short chain of case that leads to the particle's energy being completely absorbed. Methods like that of Monte Carlo was applied for the simulation of fundamental procedures in a direct manner, therefore assisted in many ways concerning medical physics. Nonetheless, these methods have not become appropriate for time-to-time treatment planning of photon beams because of the enormous demand for central processing unit (CPU) time. Centered on energy deposition kernels a partially analytical dose calculation algorithms has been established (Ahnesjö & Ahnesj, 2014). Of late, beam characterization, modeling output and adjacent (lateral) beam discrepancies have become of great importance. This gives complete understanding in relation to modeling of dose reposition, therefore facilitating planning of treatments to be approve for treatments that are more complex. Great demands of ethics for protection and quality assurance in therapy give emphasis to vital function of easy methods of dose calculation of independency checks for treatment planning systems outputs (Ahnesjö & Ahnesj, 2014).

2.1 COBALT 60 EXTERNAL RADIOTHERAPY

2.1.1 Cobalt 60 (history, decay chain, energy, half-life, activity)

The effectual use of Cobalt-60 in radiation therapy to treat and manage cancer have been in existence for over six decades (Memon et al., 2017) . Cobalt 60 isotope can be produced by exposing a metallic cobalt to neutrons of high energy, thus cobalt 60 is said to be a synthetic isotope (Thoraeus, 2017). Cobalt 60 isotope is produced by breaking Cobalt 59

into smaller forms with neutrons in a nuclear reactor as illustrated in equation 2.0 (Thoraeus, 2017).

$$^{59}_{27}Co + ^{1}_{0}n \rightarrow ^{60}_{27}Co + \gamma \ldots\ldots\ldots\ldots \text{eqn } 2.0$$

During the decay of Cobalt 60 to Nickel 60 (60-Ni), beta particle of low energy 0.31 MeV (99.8%) is emitted causing the Nickel nuclei to be unstable. To attain stability with the Nickel nuclei, two gamma radiations having 5.26 years half-life are emitted. Figure 1 below shows the decay scheme of Cobalt 60 isotope as shown in equation 2.1(Thoraeus, 2017).

$$n \rightarrow ^{60}_{27}Co \rightarrow ^{60}_{28}Ni + \beta^{-} + \gamma_1 + \gamma_2 \ldots\ldots\ldots\ldots\ldots . eqn\ 2.1$$

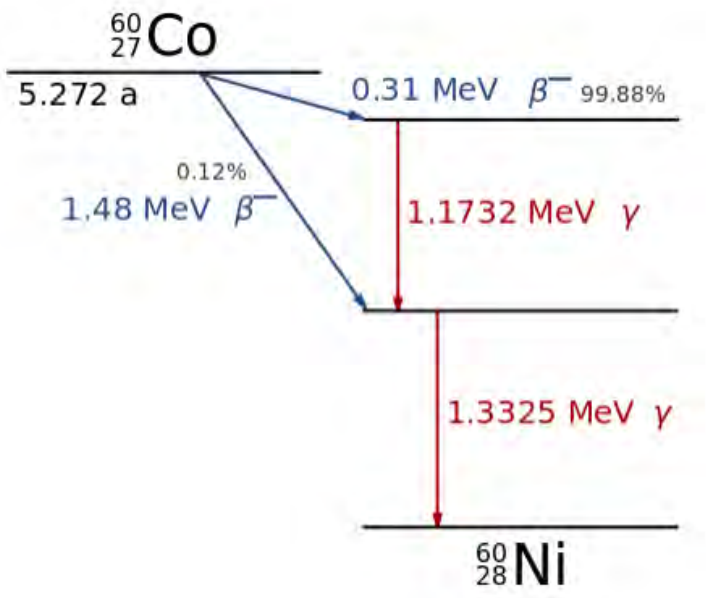

Figure 2. 1: Decay Scheme of Cobalt 60

These gamma emissions have 1.17 MeV and 1.33 MeV of energies and are used for treatment. Cobalt 60 beam is said to be monoenergetic with an average energy of the two gamma radiations being 1.25MeV (Baba et al., 2013). Cobalt 60, usually designated as Co-

60 has a neutron number of 33, proton number of 27, isotopic mass of 59.93 and a half-life of 5.27 years. Cobalt 60 has been used in place of radium since it produce gamma ray source which is of 10000 times strength of that of the radium (Thoraeus, 2017).

2.1.2 Cobalt 60 source

Cobalt 60 radionuclides build exclusively in a cylindrical capsule made of stainless steel and a twofold welded seal, which avoid any form of leakage of the radioactive material. The source is cylindrical in shape with a diameter ranging from 1 cm to 2 cm; a height of about 2.5 cm. This helps in attaining a high and sufficient activity to achieve a practical output in as much, maintaining the diameter of the source small as possible to reduce the beam penumbra. Since beam geometry of the radiation source produces a geometric penumbra since the source is not a point source. These penumbras lead to the generation of a section of dose variation at the edges of the field (Kennedy, 2001). The space at the back of the active cobalt material in the capsule need to be firmly loaded with blank discs to get rid of movement. The low energy beta radiation emitted from the source is sieved by the capsule walls (Of et al., 2016).

Cobalt 60 machines deliver moderately high-energy gamma rays used for radiation therapy that is idyllically suitable for head and neck cancers treatment as well as superficially tumours (breast cancers).These are insufficient for treating deep-seated tumours (Reddy, 1899).

During this process of gamma rays the production, the parent source goes through a beta (β) decay, producing an excited daughter nucleus, which gains ground state by emitting

gamma rays. The important and dynamic features of radioisotopes for EBRT are gamma ray with High energy, High specific activity, comparatively long half-life, large specification air kerma rate constant.

2.2 ENERGY DEPOSITION IN PHOTON BEAMS

When photons interacts with the head of a treatment machine, they emitted scattered beam which yields secondary photons component to that of primary beam in the treatment machine and in the patient before absorbing the energy is dose. Figure 2 shows the physical interaction of photons.

Furthermore, contamination of beam occurs when charged particles are release inside the head of the treatment unit and air column within the head and the medium exposed to radiation therefore adding up to the dose in the build-up region. The existence of scattering material causes the charged particle contamination to be highly responsive.

According to IAEA (1987) dosimetry protocols, calibration of beams is to be done at a depth not within the charged particle contamination range (Ahnesjö & Ahnesj, 2014). Photons do not particles directly ionize and deposit substantial energy.

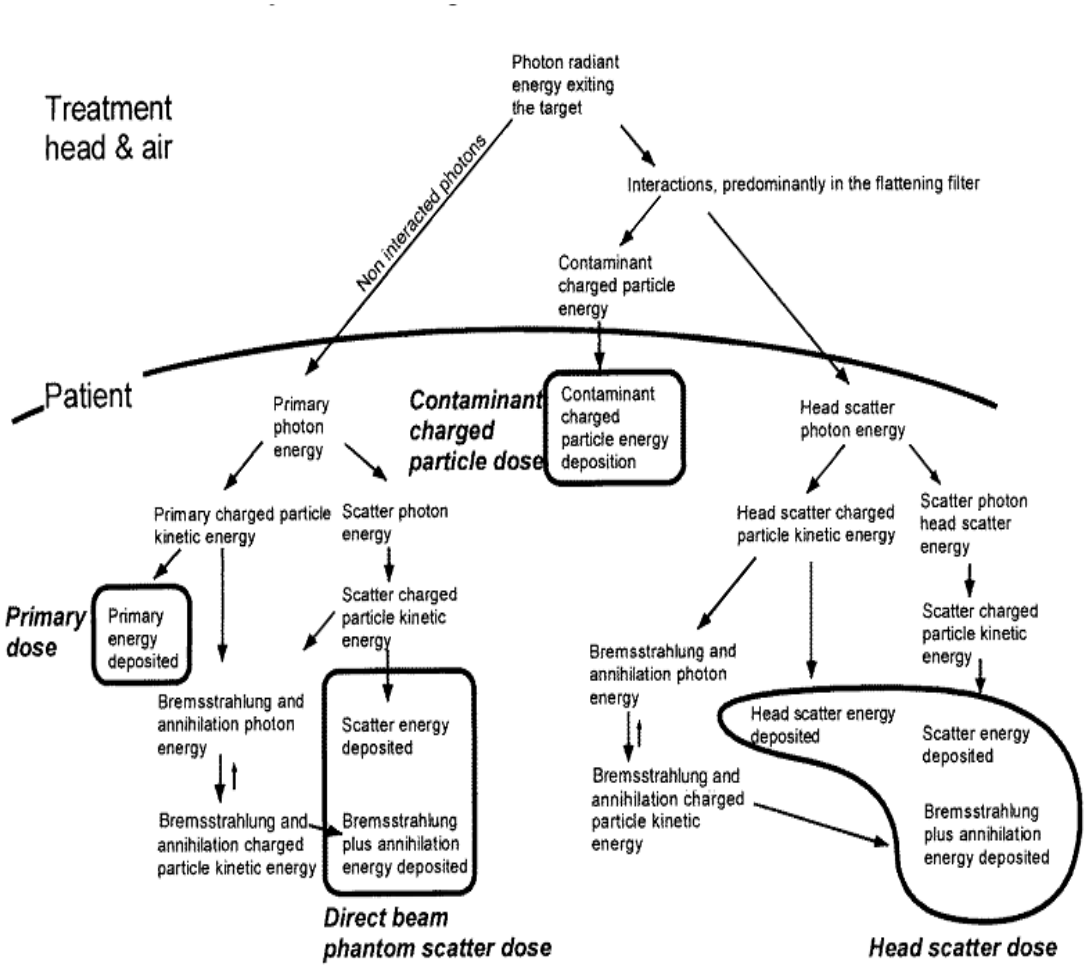

Figure 2. 2: Account of the Four-dose categories interaction: primary dose, phantom scatter dose, contaminated, charge particle dose and head scatter dose.

When photons incidents on the patient and interacts with the patient, their energy is transmitted to the electrons and positrons which ionize and excite the atoms on the paths of the particle until they totally lost their energy.

In Ahnesjo and Aspradakis (2014), by means of the interaction history, definite explanations of the different dose classifications significant to characterization of beam and modelling of dose. Beginning with electron beam target, which is the source, photons moving into the patient, is a non- interacted photon before entering the patient and this

initiates the primary scatter and distributions of phantom scatter dose. Photons which interacts within the head of the treatment machine produce double absorbed-dose elements within the patient which are the dose absorbed from indirect photons (head scatter dose) and absorbed dose from electron contamination (charged particle contamination). Reliant on energy of the beam and pattern of the treatment unit head, dose absorbed from indirect photons arising in the treatment unit head is accountable for 2 percent to 15 percent of the patient's total dose absorbed (Ahnesjo, 1995: ICRU 83, 2010).

The significance of having the idea of primary dose is because the dependency on the fluence of primary photon is local as compared to the dose liaised via scattered photons. According to the report from ICRU 42, 1987considers primary radiation as the radiation incident on phantom surface taking into accounts, the photons emitting straight from the target and radiation scattering from the beam shaping and collimating system.

2.3 THE RECIPROCITY THEOREM

It indicates that for radiation, the quantity of detected radiation do not vary by altering a point detector positions as well as a point isotropic source in an immeasurable homogeneous (Ahnesjö & Ahnesj, 2014).This theorem depicts the relationship of reciprocity concerning the primary radiation, finite volume as well the point source.

In 1945, Mayneord stated that the integral dose through all volume of finite source homogeneously repleted with material that is radioactive is equivalent to the integral dose through the original source if the receiver was repleted with radiating material of the equal unvarying density (Ahnesjö & Ahnesj, 2014). This broadens the theorem to the situation of extending both the source and the detector.

Inexplicit estimate in kernel superposition models shows that kernels are handled as infinite medium and uniform such that the theorem relates straight to superposition integrals devoid of additional approximations. Woo (1994) wrote that, even though kernels are usually deduced supposing an infinite medium, which is not a complete condition when it comes to superposition calculations, reciprocity of Kernel depicts the kernels point dose and also showing the energy deposited all over a photon interaction section. It also shows the scattering sites distribution relating to particles which facilitate energy to a dose deposition point (Ahnesjö & Ahnesj, 2014). Owing to this reciprocity, it was possible to compare the energy calculated for spread kernels to evaluate iso-line dose contribution curves (Malone and O'Connor 1989). Using this theorem in situation of polyenergetic beams where polyenergetic kernels makes it inaccurate for the reason of dissimilarities in differential energy fluence spectrum for which polyenergetic kernels are defined (Papanikolaou *et al,* 1993). Suitable planning geometries to be used in experiments is the reciprocity amongst the interaction of photons and dose deposition sites. (Ahnesjö & Ahnesj, 2014). Transport codes of radiation within adjoint mode where particles are handle by means of reverse from the corresponding section in direction of the sources employ the reciprocity (Difilippo 1998). This system is finest suitable to situation in which there is the need to evaluate small detector reaction open to great-disseminated sources.

2.4 BEAM CHARACTERISTICS

This review will discuss and give a summary on the overview of some quantities that are commonly used and defined stages alongside the central axis of a photon beam. Those

quantities are categorized in relation to the penetration characteristics of beams (depth), the effort to distinct primary dose from scatter dose as well as that, which refer to the clinical accelerator output. The three quantities, which key out the penetration characteristics of a beam, are the PDD, TMR and the TPR.

2.4.1 Penetration characteristics

Percentage Depth Dose (PDD) is a penetration characteristic of beam that describes the quotient of the dose absorbed at X and the dose absorbed at Y expressed in percentage in reference to figure 2.3. Point X can be any depth *d,* beneath the surface and the reference point Y, situated at a definite depth (*d*), beneath the surface, which is depth of maximum build-up at a point in water, both along the central axis (ICRU 24, 1976). PDD is expressed as:

$$P(d, d_0, W, s, E) = \frac{D_x}{D_Y} \times 100\% \ldots\ldots\ldots\ldots eqn\ 2.40$$

Where *d* defines the reference depth, *W* is the dimension of the field, *s* defines source-surface distance and *E is* the energy.

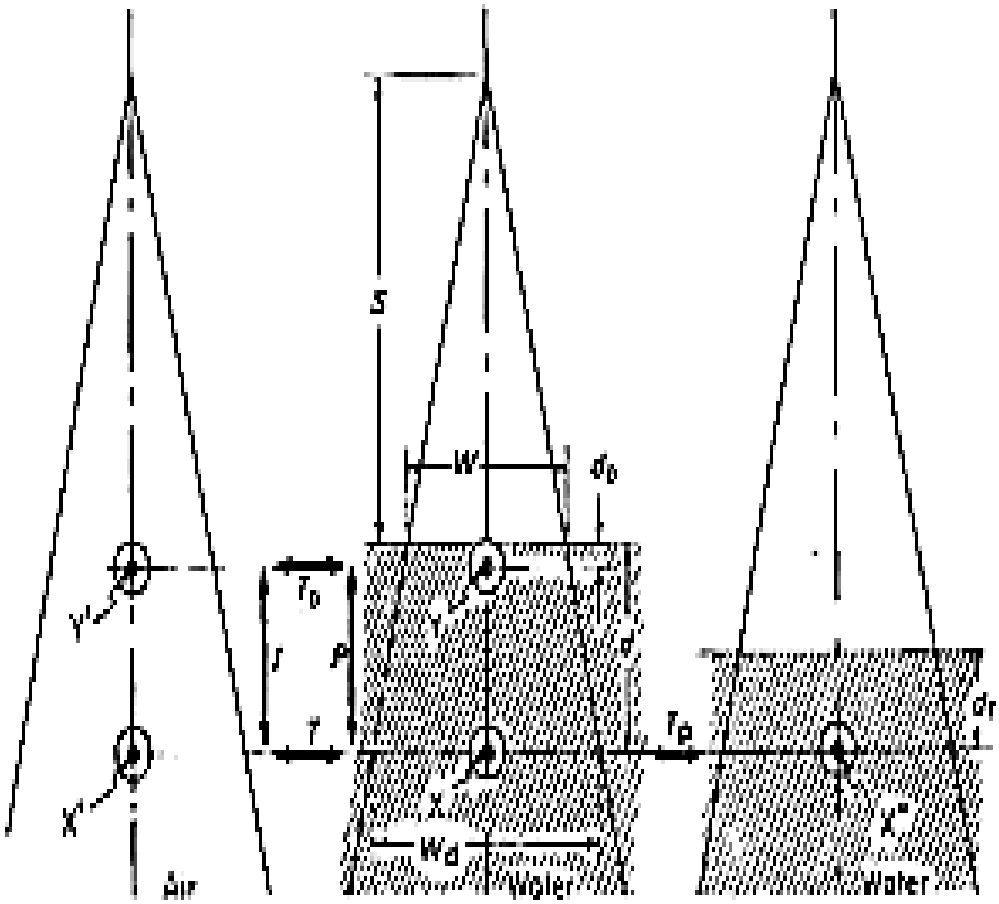

Figure 2. 3: Diagram illustrating the relation between absorbed dose use in PDD, TAR and TPR

Data from PDD are not practical for straight away reconstruction of the deliveries of dose because these data rely on the source (SSD).

According to Karzmark *et al (*1965) TPR does not dependent on SSD and it describes the fraction of the dose at X to the dose at point X" along the central axis as in Fig. 2.3. X" is at a depth of reference within a phantom *dr,* with all requirements of irradiation being constant. Also TPR can be well-defined as a quotient of the dose rate at a given point in a

water phantom and the dose rate at the same point at the normalization depth (Gibbons, et al., 2014).

The TPR quantity was specified to conform to the proposals made in the ICRU 10d, 1963 that explains that "X-ray beams should be calibrated at a reference depth in a phantom" (ICRU 1963). It depends on depth as well as field size. In condition that the depth of reference is near the range of electron contamination, the TPR possibly will differ in accordance to SSD (Gibbons et al., 2014).

$$TPR(d,\ r_d) = \left(\frac{PDD_N(d,r,SSD)}{100\%}\right)\left(\frac{SSD+d}{SSD+d_0}\right)^2 \times \left(\frac{S_p(r_{d0})}{s_p(r_d)}\right) ..eqn\ 2.41$$

TMR is the renormalization of TPR in such a way which specific depth of reference becomes the maximum dose depth. TPR is mostly preferred for dosimetry systems because of the usage of the depth of reference farther from the build-up region. TPR also avoid complications of uncertainties owing to electron contamination at the maximum depth dose, which mostly come with TMR quantity (Dutreix et al, 1997).

2.4.2 Definition of treatment machine output (ICRU 24)

Output of a treatment unit possibly will appropriately relate to a single beam evaluated for requirements that will be able to replicate freely, the rate of exposure or absorbed dose for additional requirements of importance being linked to this single measurement by determined multiplication elements. However, x-ray beams of various generator potential-filter situations cannot use the technique due to continuous steadiness of the increasing factors cannot be presume for this situation (ICRU 24, 1976).

The output of a treatment machine is the amount of the radiation beam emitted by a radiation therapy treatment machine. This is mostly referred to the rate of exposure, otherwise absorbed dose rate at a point of calibration *(q.u.)* for a strictly well-define set of circumstances. The measurement is generally done in free in air at the spatial position of the calibration point and the result is change to absorbed dose rate at the phantom surface as proposed by ICRU Report 23, 1973. For Photon energies except x-rays produced at potentials lower than 150 kV, measurement is conducted inside a phantom at a definite depth (ICRU 1976).

2.5 PRIMARY AND SCATTER DOSE COMPONENTS CONCEPT

2.5.1 Scatter dose and primary dose characteristics

Holt et al (1970) first did the parting of total output ('output in water') for the collimator (head) scatter (i.e. output in air) as well as the phantom scatter. They evaluated the total output independently from the head scatter factors, unlike phantom scatter factors (Sp) that is assess using 'field-cut' phantoms having maximum-opened jaws on the machine. Sp factors define the quotient of Scp (total scatter factor) and Sc (collimator scatter factor), thus presuming one and the same broad beam dose per energy fluence conversion of primary and head scattered photons ((Ahnesjö & Ahnesj, 2014) and (Ahnesjö, 1989)).

Dosimetric systems in the early era have attempted to dissociate scatter dose and primary dose by means of scatter factors that will show the relation of total to primary dose at a point (ICRU, 1973).

TAR is in relation with the primary dose, build-up at the maximum depth, at constant SDD. TAR describes the quotient of dose absorbed at X and the dose absorbed measured at X' with all irradiation conditions (adjustment of collimator, source distance) being constant

(refer to fig 2.3). To achieve the dose absorbed at X', the sensitive portion of the measuring instrument needs to confined by sufficient water equivalent material for extreme electronic buildup. Dose absorbed at X' is ascertained at the center of a small phantom of minimal mass free in air (ICRU 1973, 1976). TAR is expresses as:

$$T(d, W_d, E) = \frac{D_X}{D_{X,}} \ldots\ldots\ldots\ldots\ldots\ldots . eqn\ 2.51$$

Owing to investigational complications in guaranteeing perfect charged particle equilibrium in air, the meaning of TAR has been subjected to controversy and disagreements for high-energy beams. Bjarngard and Petti (1988) give a strict definition for scatter primary ratio (SPR) as a quotient of scattered dose against primary dose at a given point with the denominator, characterizing dose arising due to primary photons at a depth, which is greater as compared to the maximum build-up. SAR defines the dose absorbed arising due to scattered radiation, deduced by deducting the extrapolated value for a field of zero-area TAR from finite field TAR (Ahneson,1994).

Similarly, SMR can be evaluated by means of subtraction of the zero-area TMR from the TMR at that depth unchanged and radius of the beam. Defining both scatter air ratio and scatter maximum ratio, primary dose of maximum build-up at a depth is the denominator. Absorbed dose can be modelled out of the photons scattered by means of differentiated SAR (dSAR) that could be done by several integration methods.

Normalized peak scatter factor (NPSF), peak scatter factor (PSF) and backscatter factor (BSF) are also scatter factors. BSF describes the Scatter Phantom Ratio on the phantom surface at the central axis. It is also use for low and medium-energy X-rays. PSF occurs at a maximum build-up depth for higher-energy beams and it is described as the quotient

of the doses absorbed at points Y and Y'. In accordance with the ICRU 24 (1976), it is also recognized as backscatter factor however, for the reason that the depth (*d, u*) is finite for every photon except for low energy x-rays since it has the tendency of misdirecting (ICRU 24, 1976). The dose absorbed at Y' relates to the dose absorbed at X' by means of the inverse square law function:

$$I\,(d, d_0, s) = \frac{D_X}{D_Y} = \left(\frac{s + d_0}{s + d}\right)^2 \ldots\ldots\ldots\ldots\ldots\ldots . eqn\ 2.52$$

A considerable quantity of emission emanating from the beam collimator and other structures as well as the total beam possibly will behave as if it emitted from a virtual source in general rather closer to the surface than *s.* Though nonconformities from the inverse square relationship do not exceed one percent or two percent for generally used distances, the applicability of the correlation have to be ascertain via measurement for the requirements in use, mainly for great changes in distance. Interactions linking doses absorbed at *X, X', Y* and *Y'* in figure 4 create an ordered establishment and can move from one point to any points by two paths. For case in point, dose absorbed at *X* can be evaluated right from the absorbed dose at *Y*, with a depth dose value, otherwise, along the path: initially from *Y* to *Y'* via the inverse of TAR, then from Y' to *X'* using an inverse square factor and lastly from X' to X through another TAR (ICRU 24, 1976). Though the initial path is straight, in condition that the suitable depth dose value is unavailable, or the requirements do not correspond with the accessible data, the second path is a reasonable substitute. The process can be described by:

$$P(d, d_0, W, s, E) = \frac{T(d, W_d, E)}{T(d_0, W_{d0}, E)} \cdot \left(\frac{s + d_0}{s + d}\right)^2 \times 100 \ldots\ldots\ldots\ldots\ldots\ldots . eqn\ 2.53$$

when PSF is renormalized at a reference field size, preventing uncertainties from scattered photons, it is identified as Normalized peak scatter factors (NPSF), Ahnesjö & Ahnesj, 2014).

2.5.2 Primary and Scatter Dose

Dose delivered to a medium at a specified point contributes two components of dose to the medium that are the primary component and the scattered component. The primary component emanates directly from the source and it is independent on the field size. On the other hand, the second component is dependent on the field size and it comprises of the scatter from the collimator, flattening field and possibly air (Karlsson et al., 2010). The primary and secondary particle contributions to dose (photons and electrons) uses their effect over a different range and they are independently affected to different degrees by tissue inhomogeneities and beam boundaries. Mostly, the total dose is decomposed into two components; "primary" and "scattered" dose components. Using conventional dosimetry instrumentation, the separation has empirically been done (AAPM Report No. 85, 2004). The current Monte Carlo simulations have assisted in the demanding definition of "primary" and "scatter" separation (Woo et al., 1990) with simplified point source models being protracted to take into account the extra focal radiation (Ahnesjo, 1994; Sharpe et al., 1995). Those photons that are incident on the surface of the patient (or phantom) are characterized primary (AAPM Report No. 85, 2004).

In addition, pair production takes place when the incident photon has adequate energy (>> 1.02 MeV), to produce electron positron pairs following the production of photons of energy 0.51 MeV from positron annihilation. These photon component are referred to as

head scattered since this interactions commonly happen in structures in the head of the treatment machine (some occur in the intervening air) photons, but they still belong to the "incident" or "primary" group.

The dose from primary photons to the central axis of an open beam at depth in a phantom is dependent on distance from the source, head-scatter, which will depend upon collimator setting and other beam defining parts (block, wedges), attenuation (absorption and scattering in the phantom, determined by depth and beam energy). At any depth, the dose contribution from primary photons is determined by the collimator setting, and not by the size of the radiation field at that depth (Dutreix, 1997).

The first time such photons interact with the medium, they contribute to primary dose through recoil electrons (AAPM Report No. 85, 2004). The dose deposited by photons that have formerly interacted in the medium (at least once) is termed the scattered component of the dose. The scattered photons is dependent on the energy of the photon and the volume (field size, depth, and patient thickness) of patient being irradiated The total dose along the central axis can then be decomposed into:

$$D\ (x,r) = Dp\ (x) + Ds\ (x,r) \ldots\ldots\ldots eqn\ 2.53$$

where *r* refers to the radial distance to the field edge.

The primary dose is isolated by an extrapolation of the dose as against field size curve to a small pencil beam field size. The restriction of the selected field size will define whether the primary component comprises or ignores the primary electrons. This had led to the ambiguous definition of a "pencil beam" (Bjarngard and Petti, 1988; Woo et al., 1990). A decrease in the photon fluence and the electron fluence produced by the primary dose component are the two (2) effects that concurrently decrease the central dose (AAPM

Report No. 85, 2004). Principally primary dose is related to the primary collision KERMA, deposited from charged particles that are set in motion by only the primary photons. The scatter dose is characterized by all secondary radiations, as well as Compton scattered photons, annihilation photons, and bremsstrahlung. Using the reciprocity theorem (Johns & Cunningham, 1983) the contribution from each component is simply the summation of all pixel values in each dose-spread image (AAPM Report No. 85, 2004).

2.6 CENTRAL AXIS DEPTH DOSE.

To characterize the Central axis depth dose within a medium, percentage depth dose is standardized to D_{max} (100%) at the maximum dose depth, d_{max} that is expressed as;

$$P\ DD(d, A, f, hv) = \frac{DQ}{DP} = \frac{DQ'}{DP'} \ldots\ldots\ldots\ldots\ldots\ldots eqn\ 2.60$$

DQ and D˙Q represent the dose and dose rate at the point Q at a given depth d on the central axis within the phantom in reference to figure 2.5 below. DP and D˙P represents the dose and dose rate at the point P (at d_{max}).

The depth dose behaviour of photon beams in a medium can be estimated taking into account different parameters, which show the attenuation in its primary intensity. The absorbed dose is generally defined as Percent Depth Dose, which is a function of depth ***d***, field size ***r*** and Source to Surface Distance (SSD) ***f***. Therefore, the dose at the point Q is contributed by two components (primary and scattered) is expressed as:

$$PDD(d, A, f, hv) = 100\left(\frac{f + d_{max}}{f + d}\right)^2 e^{-\mu_{eff}(d - d_{max})} \cdot K_s \ldots\ldots\ldots\ldots eqn\ 2.61$$

Where f is the source to surface distance (SSD), d is the depth for the SSD, d_{max} is the maximum depth and μ_{eff} is the effective linear attenuation coefficient.

The Primary component of the PDD function that accounts for the primary dose in equation 2.61 is

$$PDD(d, A, f, hv) = 100\left(\frac{f + d_{max}}{f + d}\right)^2 e^{-\mu_{eff}(d-d_{max})} \ldots\ldots\ldots\ldots . eqn2.62$$

Ks is the scattering component of the PDD function that accounts for the change in the scattered dose and can be determined by the expression below;

$$K_s = \frac{PDD(d, A, f, hv)}{\left[100\left(\frac{f + d_{max}}{f + d}\right)^2 e^{-\mu_{eff}(d-d_{max})}\right]} \ldots\ldots\ldots\ldots\ldots\ldots\ldots\ldots\ldots eqn\ 2.63$$

This point out the three governing rules of photon beam attenuation, inverse square law, exponential attenuation, and scattering component Ks. This is why Percent Depth Dose uniquely varies with depth due to attenuation, with SSD due to inverse square law, and with field size due to scattering effect (Budzar et al., 2009).

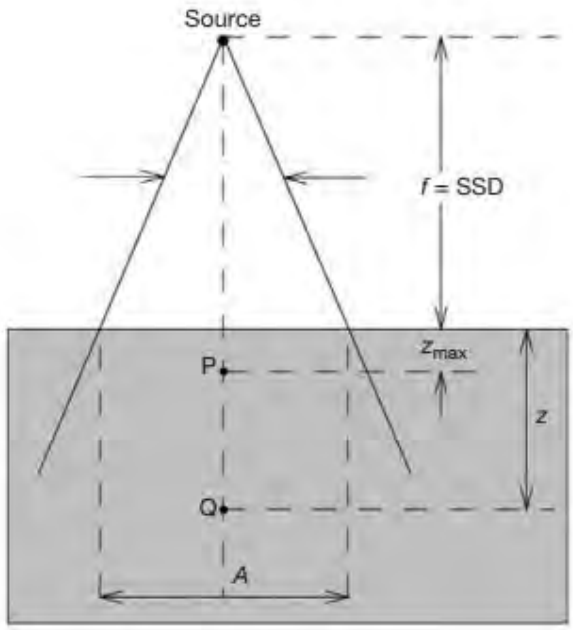

Figure 2. 4: Shows the setup measurement for PDD

2.6.1 Characteristics of central axis depth dose distribution

Various features that describes the central axis depth dose distribution includes near surface dose, dose build-up of secondary electron usually to some extent contaminating and secondary photons. Other characteristics are primary electrons dose build-up because of an increment in the inclining tracks, maximum dose in which electrons approaches complete diffusion, the increase loss of primary electrons with descending section, the step part of the decrease in linear dose owing to range straggling of the primary electron and energy.

2.7 DOSE MODELLING.

The inverse square law, attenuation of the primary beam, the build-up of photon generated electron fluence (few cm depth) and build-up of phantom scatter dose (9 to 18

cm depth), and electron contamination from sources within the treatment head and in the air between the treatment head and the patient are the four major physical phenomena, which contribute to the establishment of depth dose distributions in water (Karlsson et al., 2010). Interaction of High-energy photons with matter causes indirect ionization to release charged particles (electrons or positrons) that deposit energy through Coulomb interactions with orbital electrons of the atoms (Pacyniak, 2016). The intensity of a monoenergetic photon beam, Ip, incident on a medium attenuates according to the exponential law is expressed as:

$$I_p(x) = I_o e^{-\mu x} \ldots\ldots\ldots\ldots\ldots\ldots\ldots eqn\ 2.70$$

Io represents the initial photon intensity, μ linear attenuation coefficient for the medium at depth, x. this expression characterizes the primary component of the photon beam. The linear attenuation coefficient μ is the summation of the attenuation coefficients of several interactions,

$$\mu = \tau + \sigma_R + \sigma_C + \kappa \ldots\ldots\ldots\ldots. eqn\ 2.71$$

where τ is the photo-electric coefficient effect, σR , the Rayleigh scattering, σC , the Compton scattering and pair productions κ. Compton scattering is the most significant interaction in the therapeutic range that leads in the energy range of 6 to 18 MV X-rays (Pacyniak, 2016).

Figure 2.5 shows a depth dose curve is with the dose separated into these components. The part of the dose that is due to photons scattered in the treatment head, i.e. the indirect part of total beam fluence, is shown separately as head scatter dose. This part can also be subdivided into a primary part and a phantom scatter part, depending on how the dose

calculation model treats these parts (Karlsson et al., 2010).

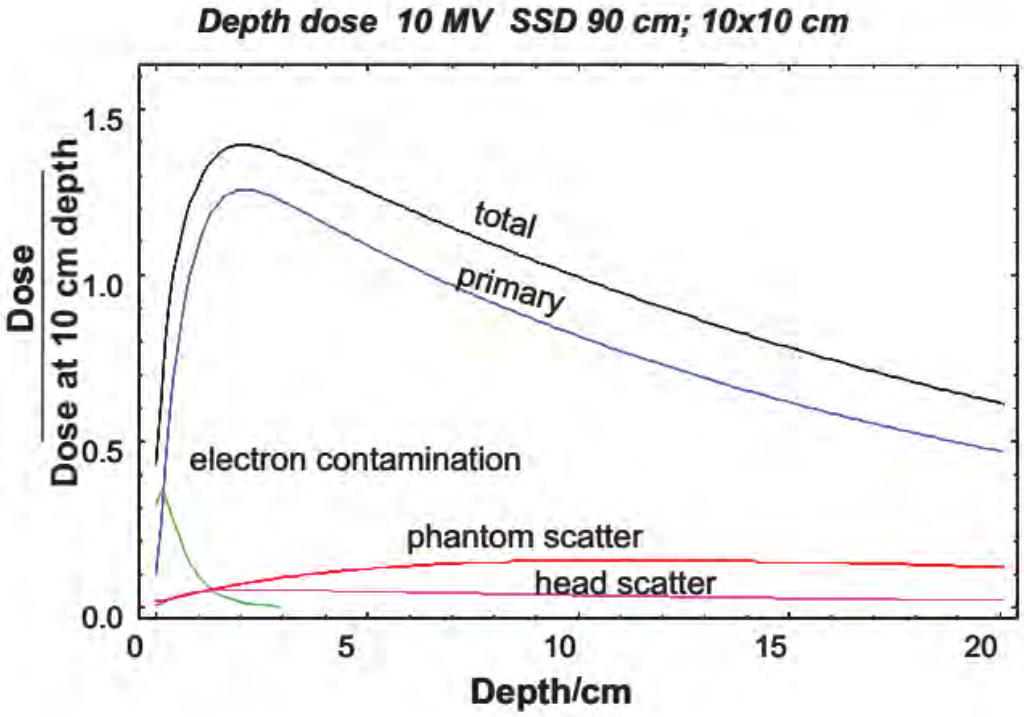

Figure 2. 5: shows a depth dose curve is with the dose separated into these components.

The pure effect of treatment distance is the inverse square law that is not dependent of the shape and size field making it very simple to factorize. This defines Tissue Phantom-Ratio (TPR) that is referred to as the relative depth dose distribution for a non-divergent (infinite SSD) field (Karlsson et al., 2010). The dose deposited by electrons freed from the initial interaction of each photon entering the medium is termed the primary dose of the medium and its depth distribution is complies with the primary fluence attenuation distribution for depths which are larger than the buildup depth with the condition that the field size is large enough to develop lateral electron equilibrium. The least field size necessary for lateral electronic equilibrium is dependent on the following; primary beam spectrum, the projected source size, and the composition of the irradiated medium. Therefore,

calculations of lung dose need more attention because the lateral disequilibrium transpires for field sizes four to five times larger than in water (Karlsson et al., 2010). On the other hand, the scatter component of the dose depends on the primary beam spectrum, the shape and size of the field. According to Ahnesjö et al (1992) and Nyholm et al. (2006), the scatter depth dose distribution attains its maximum in water at the order of 9 to 18 cm (Ahnesjö et al., 1992b; Nyholm et al., 2006c) and is therefore very differently shaped from the primary dose distribution (Karlsson et al., 2010).

2.7.1 Correction for tissue inhomogeneities

Tissues of different types and density have effect on the dose deposition inside a patient and this effect is dependent on the volume, density and atomic number of the inhomogeneities. If the area of the importance is found in front of the inhomogeneities then the dose is merely affected. On the other hand, the dose is predominantly affected when the locale is found within the inhomogeneities because of the changes in the secondary electron fluence (not as much in the primary beam attenuation). The dose is predominantly affected by the primary beam attenuation for locales beyond the inhomogeneities. Some empirical approaches can be used to correct the dose in inhomogeneities (Hudej, 2008).

2.8 BEAM MODELLING AND DOSE CALCULATIONS

There are various approaches of different dose calculations and it is a compromise between the advantages and downsides associated with different methods of calculation

prior to accuracy, speed, simplicity of use. The intricacy of present external beam therapy (EBRT) modus operandi and the demands on clinical efficacy needs methods of dose calculation that provide a high degree of generalization, simplification and healthy to use By tradition, factor-based calculation have been employed where dose calculation is performed through sequence and series of multiplicative correction factors, which define the modification and alterations in dose, related with the alteration of an individual treatment parameter, like the field size and depth. This approach has been the subject of detailed descriptions (Venselaar et al., 1999; Dutreix et al., 1997). The individual factors are normally structured in tables derived from measurements or described through parameterizations and other factors are calculated through simple modelling, (for example the inverse square law accounting for varying treatment distances) (Karlsson et al., 2010). When required data are available, the factor-based method may possibly be a smart method owing to its computational simplicity, considering the implementation point of view. The related difficulty with this approach is the needed amount of data from commissioned beam since the approach cannot calculate doses when the beam setup is not covered by the commissioned set of data. Relating to treatment modus operandi, which involve the application of many degrees of freedom (the shape of an irregular field) it becomes virtually not possible to tabularize all factors required for all conceivable (Karlsson et al., 2010).

Therefore, the factor-based approach is appropriate for point dose calculations along the central beam axis in beams of simple (rectangular) shapes. Monte Carlo simulation is presently the common available dose calculation technique. The approach plainly simulates the transportation of particle and energy deposition through

probability distributions, detailed geometric accounts and data from fundamental interaction of radiation cross-section (Karlsson et al., 2010).

2.8.1. Model based algorithms

Dose distribution within the patient can be calculated using the Model based algorithms directly by modeling the beam and beam interactions with the medium (Karlsson et al., 2010). The calculation of dose distribution (in 3D) takes into consideration both the primary and scattered components of radiation that is individually considered through the volume of the tissue (Karlsson et al., 2010). This approach is to a certain extent difficult since the primary source is in general composed of a continuum of various particles that do not come from the same point and scattering within the patient is in no way simpler and this compromises between accuracy and speed (Hudej, 2008.).

2.8.2 Superposition principle

For this method radiation is decomposed into primary and scattered contributions.

The advantage is that each component can be separately adjusted to the beam shape, intensity, surface topology and internal tissue densities (Hudej, 2008).

2.9 QUALITY ASSURANCE

Quality assurance (QA) during the radiation therapy treatment planning process is mandatory to minimize undue exposure, and beam dosimetry of 60-Co teletherapy units is

an essential QA procedure, as described in the IAEA Technical Documents (IAEA TECDOC-989, 1997).

2.9.1 Recommended QA for cobalt-60 unit

In radiation therapy, QA is defined as 'all procedures that ensure consistency of the medical prescription, and the safe fulfilment of that prescription, as regards the dose to the target volume, together with minimal dose to normal tissue, minimal exposure of personnel and adequate patient monitoring aimed at determining the end result of the treatment' (Podgorsak, 2005:407; WHO, 1988). According to Fogarty et al. (2001), an effective quality assurance strategy for radiation therapy must reassure that obligatory principles and criteria are met otherwise; corrective action must be put in place based on knowledge about the errors (uncertainties) and their consequences.

According to Peiffert et al (2007), the errors acquired in the process of radiotherapy are difficult to identify retrospectively since the effects typically appear a long time after the radiation treatment delivery and because the symptoms can be diffuse and be similar to problems common also after delivery of correct radiation treatments (Peiffert et al., 2007). The examination of treatment errors can expedite the formulation, introduction and/or adoption of QA procedures to overcome their occurrence (Thwaites et al., 1995). It aids the staff in charge to bring up to date their knowledge in QA procedures and develop new methods in QA, therefore enhancing the work practices of the department (Peiffert et al., 2007). Repetitive QA on cobalt-60 is necessary to observe the stability of its performance so that any errors can be detected as early as possible. Cobalt-60 QA consist of several

mechanical tests, safety interlocks, and dosimetry consistency checks (IAEA, 2008: AAPM Task Group 40, 1994; Thwaites et al. 1995 & 2005).

Mechanical tests involve reviewing the accuracy of various physical components of the cobalt-60 such as cross-hair alignment and the coincidence of the light and radiation fields and laser alignment need to be within 2mm (Thwaites et al. 2005; IAEA, 2008).

Other checks include safety interlocks, which involve checking the functionality of various safety control systems such as door interlock and emergency switch; dosimetry consistency involves calibrating various dosimetric parameters such as radiation output and properties of beam modifiers (Dunscombe et al., 2007; Thwaites et al., 2005).

Equinox Cobalt-60 QA practices were found to be in place at the study the unit was still under warranty with once a year maintenance contract by the manufacturer.

CHAPTER THREE

MATERIALS AND METHODOLOGY

3.0 INTRODUCTION

This chapter outlines the materials and methods used in this research study. This chapter will discuss into details, the procedures that was carried out in this research study. In addition, the materials used in the research study will be discussed.

3.1 MATERIALS

3.1.1 Theratron Equinox 100 Cobalt 60 teletherapy unit

The Theratron Equinox 100 Cobalt 60 teletherapy unit, as shown in Figure 3.1, was used for radiation therapy at the NCRNM, KBTH. This unit was manufactured by Theratron in April 2013 and acquired from Canada with a model number 2117. A rotatable gantry and collimator lead the Equinox teletherapy unit. It works with a unit head panel, hand control and control console with display monitor.

The head of the treatment was isocentrically mounted with source to axial distance (SAD) of 100 cm and it consists of a double encapsulated cobalt 60 source with an initial total source activity of 399.0 TBq that was measured on 1st August 2013 by the manufacturer of the source (Nordion Inc. Canada). This treatment machine has a reference beam output in water at the depth of maximum dose ($d_{max} = .05\ cm$) of 189.49 cGy/min (on December 12, 2013), measured after installation of the telecobalt machine, According to the

International Atomic Energy Agency (IAEA) technical series report (TRS) 398, (2000) protocol (IAEA TRS-398, 2000). It has beam quality specifier for megavoltage beams of 58.36 % that is the Percentage depth dose (PDD) for the reference field size of 10 cm x 10 cm for a depth of 10 cm in water (PDD_{10}).

The Cobalt 60 source is categorized as C-146 teletherapy source capsules (by Canadian Nuclear Safety Commission High) with a diameter of 2 cm and length of 4 cm, and it is embedded in a source drawer mechanism that uses a pneumatic system to bring the source in and out of treatment position.

In the course of treatment, the radioactive source, Cobalt-60 is moved from a shielded safe positioned inside the gantry (safe position of a double layer stainless steel capsule with the diameter of 2.0 cm and 4.0 cm long of the whole source assembly) and brought in the collimator position.

The teletherapy unit is a modern computerized system with a Prowess Panther treatment planning software that runs on a Microsoft Windows computer and is configured according to the specific regional setting. This software uses computed tomography image slices to estimate doses according to physician contour drawings, which in turn is used for planning by medical physicists.

Figure 3. 1: Theratron Equinox 100 Cobalt 60 teletherapy unit

3.1.2 Cylindrical Ionization Chamber

A cylindrical ionization chamber (shown in Fig. 3.2) with volume: 0.125 cc was used for this study. The chamber was manufactured by PTW Freiburg, Germany with Serial number Tw31002-0393 manufactured the chamber. The ionization chamber is made with Acrylic PMMA with a build-up cup of thickness 3 mm. It was calibrated against a source of known beam quality at the IAEA Secondary Standard Dosimetry Laboratory (SSDL). The calibration was done with a bias voltage of 230 V at the temperature of 20° c and pressure of 101.325 kPa.

Figure 3. 2: Cylindrical Ion Chamber

3.1.3 2-Dimensional Water phantom

An in-house manufactured manual two-dimensional (2-D) water phantom was used for this research study (Figure 3.3). The phantom was manufactured from poly-methyl methacrylate (PMMA) material, for teletherapy experimental work **(AAPM TG 106).** The phantom is constructed in such a way that scatter is minimized to a greater degree.

The phantom has a height graduation reader, which helps in the depth readings. The phantom was used to measure the transit time dose to water at different depths and different field sizes

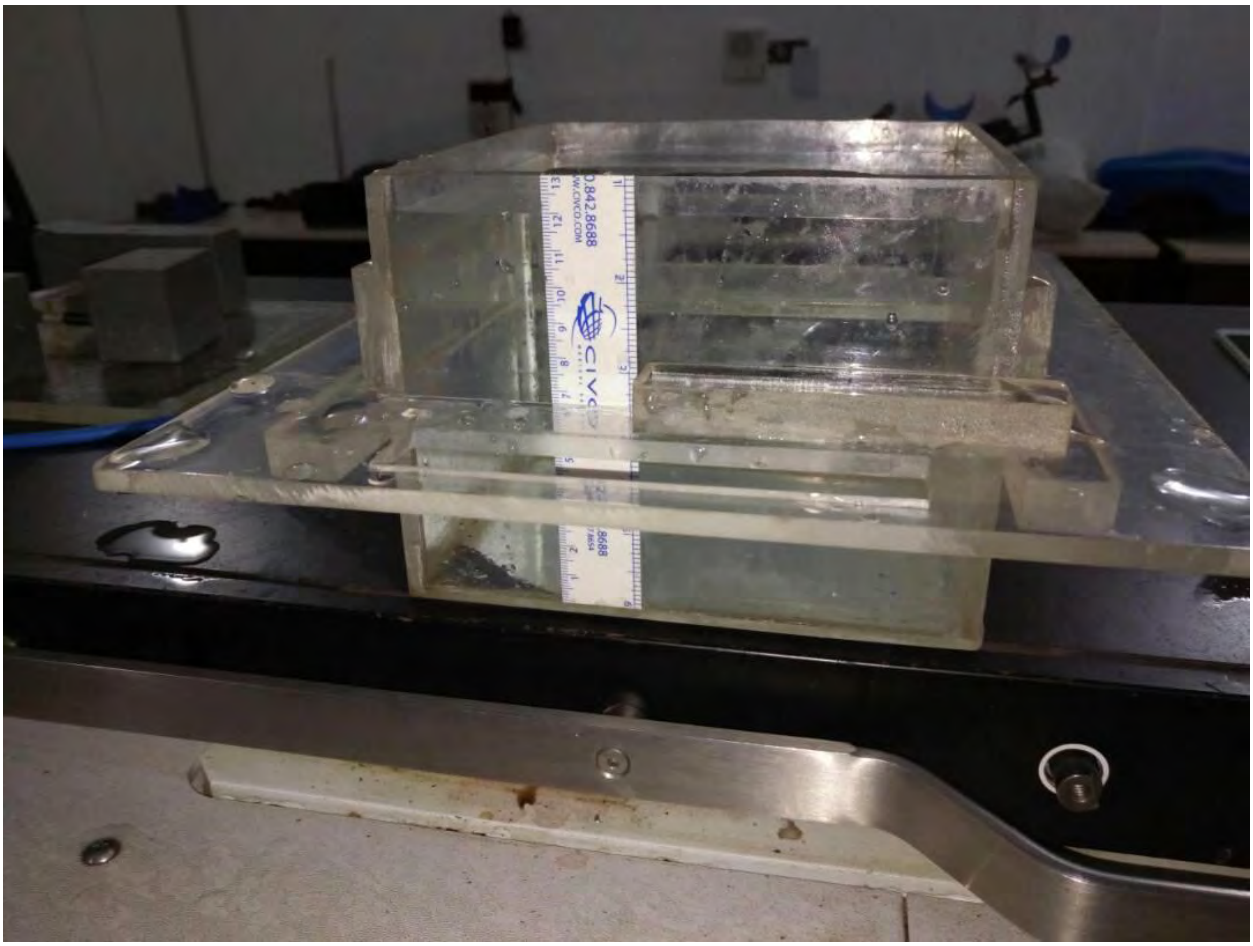

Figure 3. 3: In- house 2-Dimensional Water phantom

3.1.4 Electrometer

The PTW UNIDOS electrometer (Freiburg, Germany) with serial number T10002-20204 is a high performance secondary standard and reference class electrometer used universally for either radiological or electrical measurements. The electrometer shows measured values of dose, dose rate, electric charges and electric currents. Values of dose and dose rates are measured in gray (Gy), Sievert (Sv), Rontgen (R), gray per minute (Gy/min), Sievert per hour (Sv/hr) or Rontgen per minute (R/min) whiles those of electrical charges and currents are measured in coulomb (C) and ampere (A) respectively. Figure 3.4 shows the PTW UNIDOS electrometer used for this study.

Figure 3. 4: Electrometer

3.1.5 Digital Thermometer

EXTECH instrument 39240 waterproof thermometer with 70mm stainless steel stem was used for measuring temperature of water in the phantom during the study. As presented in Figure 3.5, it has a temperature range of -40 ^{0}C to 200 ^{0}C, resolution of 0.1^o and ±1 ^{0}C/+2 ^{0}F accuracy.

Figure 3. 5: Digital Thermometer

3.1.6 Barometer

Prazision barometer with model number 98889 compensiert (manufactured in Germany) was used to determine the pressure in the study. This is shown in the Figure 3.6 below

Figure 3. 6: Barometer

3.1.7 Software

The Microsoft excel software (2013) produced by Microsoft Corporation was used for the compiling of the data into tables and the drawing of the graphs used in this work. It is a high performance spreadsheet analyzer for technical analysis. It enabled the determination of gradients and various intercepts of the graphs and created mathematical solutions for various equations used in the completion of this project.

3.2 METHOD

3.2.1 Experimental set up and data collection

3.2.2 Determination of the Effective Linear Attenuation Coefficient

Before the whole procedure started, the reference temperature and pressure in the room was checked and recorded as 20 degree Celsius and 101.325 kPa respectively. An in-air measurement with the build-up cup was done using a source to detector distance of 100-cm. The cylindrical ionization chamber was set in the path of the beam isocentrically. The readings of the ionization chamber were obtained by placing an empty water tank (height of 0 cm) in the jaws the Cobalt 60 machine. A field size of 25 by 25 centimeter square was set, verified and confirmed.

With the electrometer set to a 60 second responds time, the Cobalt 60 source was used to irradiated the empty tank after which the electrometer reading was recorded.

This procedure was repeated for field sizes of 20 cm x 20 cm, 15 cm x15 cm, 12 cm x12 cm, 10 cm x10 cm, 8 cm x 8 cm, 6 cm x6 cm, 4 cm x4 cm and 2 cm x 2 cm.

After the first phase of the procedure, the water tank was then filled with water to a height of 2 cm and was irradiated after a field size of 2 cm x 2 cm was set, verified, confirmed.

Using the same height of water (2 cm), the procedures were repeated for field sizes of 4, 6, 8, 10, 12, 15 and 20. The procedures were repeated for varying depths of 4, 6, 8, 10 and 12 cm (increment of 2 cm) for each field size. After each irradiation for a particular depth of water and field size, the initial and final temperatures as well as the pressure were accordingly checked and recorded.

Figures 3.7a and 3.7b illustrated below show the set-up for the research study.

Set up

Figure 3. 7a: showing the whole set-up of the procedure used

Figure 3. 8b: showing the whole set-up of the procedure used

3.3 DATA ANALYSIS

3.3.1 Correction for electrometer reading

Temperature and pressure were corrected using the data collected and equation below;

Reference temperature =20 degree Celsius

Reference Pressure =1011.325 kPa

Final Pressure =101.15 kPa

Correction for temperature and pressure

$$K_{cor} = \left[\left(\frac{273.15 + T_f}{273.15 + 20}\right) \times \left(\frac{101.35}{101.15}\right)\right] \ldots\ldots\ldots\ldots\ldots eqn\ 3.0$$

Correction for readings

$$M_{cor} = K_{cor} \times Av.\ reading \ldots\ldots\ldots\ldots\ldots\ldots\ldots\ldots\ldots eqn\ 3.1$$

$$M_{cor} = \left[\left(\frac{273.15 + T_f}{273.15 + 20}\right) \times \left(\frac{101.35}{101.15}\right)\right] \times (readings) \ldots\ldots eqn\ 3.12$$

$$corrected\ reading = \left[\left(\frac{273.15 + T_f}{273.15 + 20}\right) \times \left(\frac{1011.35}{101.15}\right)\right] (readings) \ldots\ldots eqn\ 3.13$$

3.3.2 Linear Attenuation Coefficient (μ)

When photons incident on a homogeneous medium of density ρ, they attenuate steadily with each centimeter of the media attenuating at a constant fraction of the initial intensity. Consequently, the intensity function on the exponential decay law of equation 2.90 (refer to chapter two).

The primary effect of photons is to 'knock out' electrons from the cell material. The energy lost by the photons is transformed into ionization energy. These ionization electrons or electron fluence are proportional to absorbed dose from which the central axis percentage depth dose is derived (Pacyniak, 2016).

To determine the percentage depth dose, there was the need to, first determine the linear attenuation coefficient of water in relation to equation 2.62 (refer to chapter 2).

Considering equation, $I_p(x) = I_o e^{-\mu x}$ and taking ln on both sides of equation yielded

$$\ln(I_p) = \ln(I_0) - \mu.x \ldots\ldots\ldots\ldots\ldots\ldots eqn\ 3.16$$

Where

$$\ln(I) = ln\left[\left(\frac{273.15 + T_f}{273.15 + 20}\right) \times \left(\frac{101.35}{101.15}\right)\right] * (readings) \ldots\ldots\ldots\ldots eqn\ 3.17$$

and x is the height (depth in cm) of the water in the tank

A graph of $\ln(I)$ was plotted against x cm to determine the linear attenuation coefficient μ, of water.

3.3.3 The Effective Linear Attenuation Coefficient(μ_{eff}).

An expression for the calculation of the effective linear attenuation coefficient μ_{eff} (for the varying field sizes) was obtained from the equation displayed on the plotted graph of the linear attenuation coefficients of water obtained (for the various field sizes) against one side of a square field are shown in the figures at the appendix S, figure 5.

From the plotted graph, the expression below was obtained for the effective linear attenuation coefficient μ_{eff} calculations.

3.4 DETERMINATION OF THE PRIMARY FUNCTION (PDD_{pri}) OF THE PERCENTAGE DEPTH DOSE (PDD) FOR EACH FIELD SIZE

Data;

Source to surface distance, SSD = 100 cm

d_{max} = 0.5 cm

Height of water (depth cm) d = 2 cm, 4 cm, 6 cm, 8 cm, 10 cm, 12 cm.

Effective linear attenuation coefficients μ_{eff} are the estimated values in table 4.2 in chapter 4.

By substituting for the necessary data, the primary component of PDD was determined using equation 2.63 in chapter two.

3.5 DETERMINATION OF THE SCATTERED FUNCTION (K_s), OF THE PERCENTAGE DEPTH DOSE (PDD)

To obtain the scattered component K_s, of the PDD, a ratio of the measured PDD component that was obtained from the Korle – Bu Teaching hospital, Radiotherapy center and the calculated primary PDD components were determined for each field size at a specific depth. From equation 2.61 $PDD(d, A, f, hv) = 100\left(\frac{f+d_{max}}{f+d}\right)^2 e^{-\mu_{eff}(d-d_{max})}$. K_s (in chapter two), the scattered component K_s, was estimated.

$$Scattered\ component\ (PDD) = \frac{measured\ component(PDD)}{Primary\ component\ (PDD)} \ldots\ldots eqn\ 3.2$$

$$\Longrightarrow K_s = \frac{PDD(z, A, f, hv)}{\left[100\left(\frac{f+z_{max}}{f+z}\right)^2 e^{-\mu_{eff}(z-z_{max})}\right]} \ldots\ldots\ldots\ldots\ldots\ldots\ldots\ldots\ldots eqn\ 3.3$$

3.6 DETERMINING AN EQUATION FOR THE SCATTERED FUNCTION K_s, OF THE PERCENTAGE DEPTH DOSE (PDD)

To establish an expression for K_s, a graph of the generated K_s, was plotted with respect to the field sizes using Microsoft excel, which generated an equation for the line of best fit and the equation can be expressed as:

$$y = aln(d) + b \ldots\ldots\ldots eqn\ 3.3.$$

where 'a' and 'b' are constants, d is the depth (cm) and y is the scatter component.

3.7 DETERMINING CONSTANTS 'a' AND 'b'

The constants 'a' and 'b' were obtained from the equation of the line of the plotted scattered function. These constants were determined for all the field size. Furthermore an expression was obtained for 'a' and 'b' by plotting graphs for both constants.

CHAPTER FOUR

RESULTS AND DISCUSSION

4.0. INTRODUCTION

This chapter discusses the obtained results from the procedures outlined in chapter three as well as the statistical analysis and findings

4.1 ANALYSIS OF RESULTS AND DISCUSSION

4.1.1 Linear attenuation coefficient of water

From the recorded measurements, the data of readings corrected for temperature and pressure with respect to the readings from the ionization chamber response can be found in Appendix A for all the depths and field sizes used in this research study. The graphs for the plotted corrected readings against depth d, can also be found in Appendix O. An equation for each field size was established with a Microsoft Excel algorithm as shown in Figure 4.1(similar process was followed for the other field sizes). Because the corrected electrometer reading *ln (I)* is directly proportional to the depth d, a straight-line graph was generated.

Figure 4.1 represent the plotted graph of the of $\ln(I) = \ln(I_0) - \mu x$, where the ordinate is the readings obtained from the response of the ionization chamber corrected and the abscissa is the height (depth) in centimeters of the water in the phantom for a particular field size.

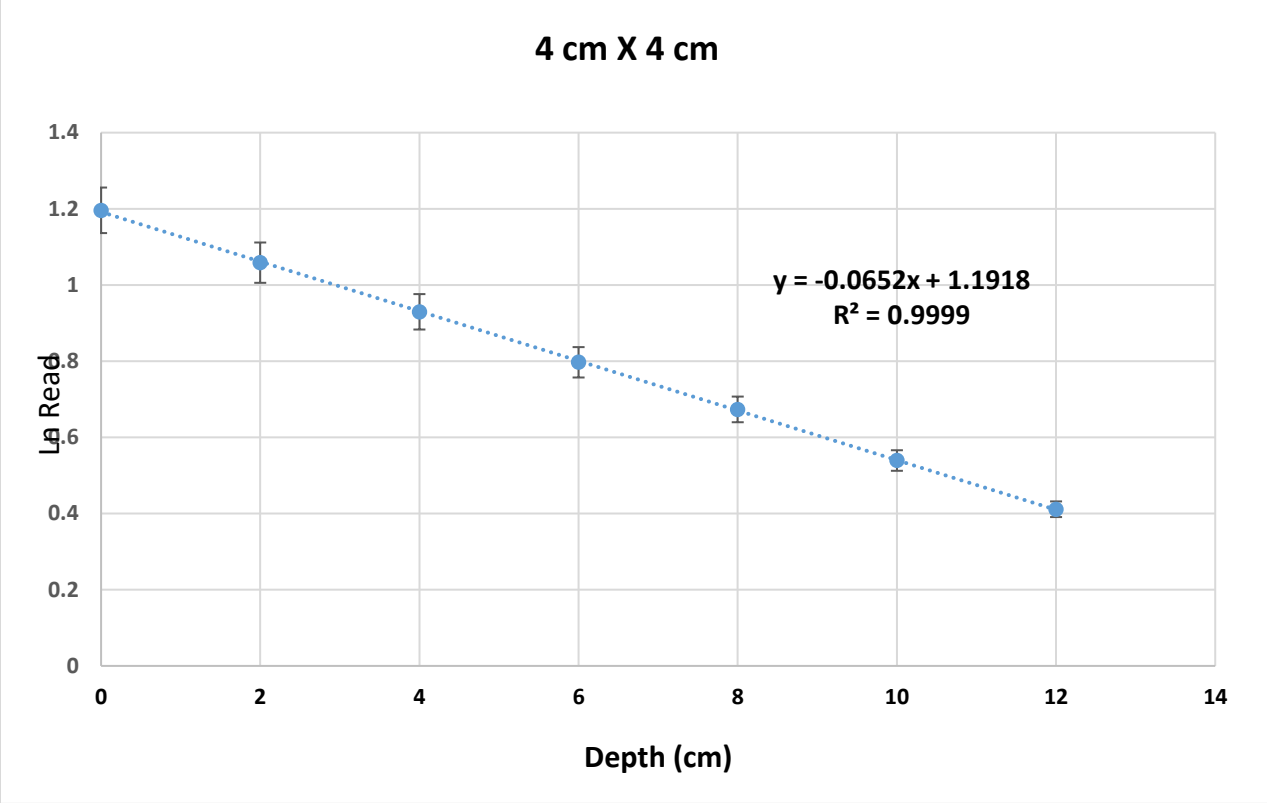

Figure 4. 1: Shows a graph of ln(I)=ln(I_0)-μx was plotted against x(cm) to obtain the linear attenuation coefficients of water for (4×4) cm^2 field size.

From the graph the linear attenuation coefficient for water, $\mu = 0.0652\ cm^{-1}$ (the gradient of the line) at d_{max} in a $4\ cm \times 4\ cm$ field with an intercept, $ln(I_0) = 1.1918$ and $R^2 = 0.9999$ respectively. The linear attenuation coefficient obtained is comparable to the LAC of water ($0.0657\ cm^{-1}$) as stated by Khan (2010).

The linear attenuation coefficient was need for the determination of the effective LAC with respect to each field size. Table 4.1 show the linear attenuation coefficients of water obtained for the various field sizes.

Table 4. 1: Table of one side of a square field against LAC (cm-1) for cobalt 60 in water.

One side of a square field (cm)	Linear Attenuation Coefficient (cm^{-1}) (H_2O)
4	0.0652
6	0.0649
8	0.0645
10	0.0639
12	0.0633
15	0.0621
20	0.060
25	0.0572

4.4.2 Effective linear attenuation coefficient

Figure 4.2 indicate the plot of LAC (cm^{-1}) against one of a square field size (cm). A polynomial fit of the second order resulted in an equation of the line,

$$y = -1E-05x^2 - 8E-05x + 0.0657 \ldots\ldots\ldots\ldots eqn\ 4.0$$

where x is the field size

y is the effective linear attenuation μ_{eff}

for the field size of 4x4, with $R^2 = 0.9997$ as shown in the graph 4.1 below, using the obtained LAC's.

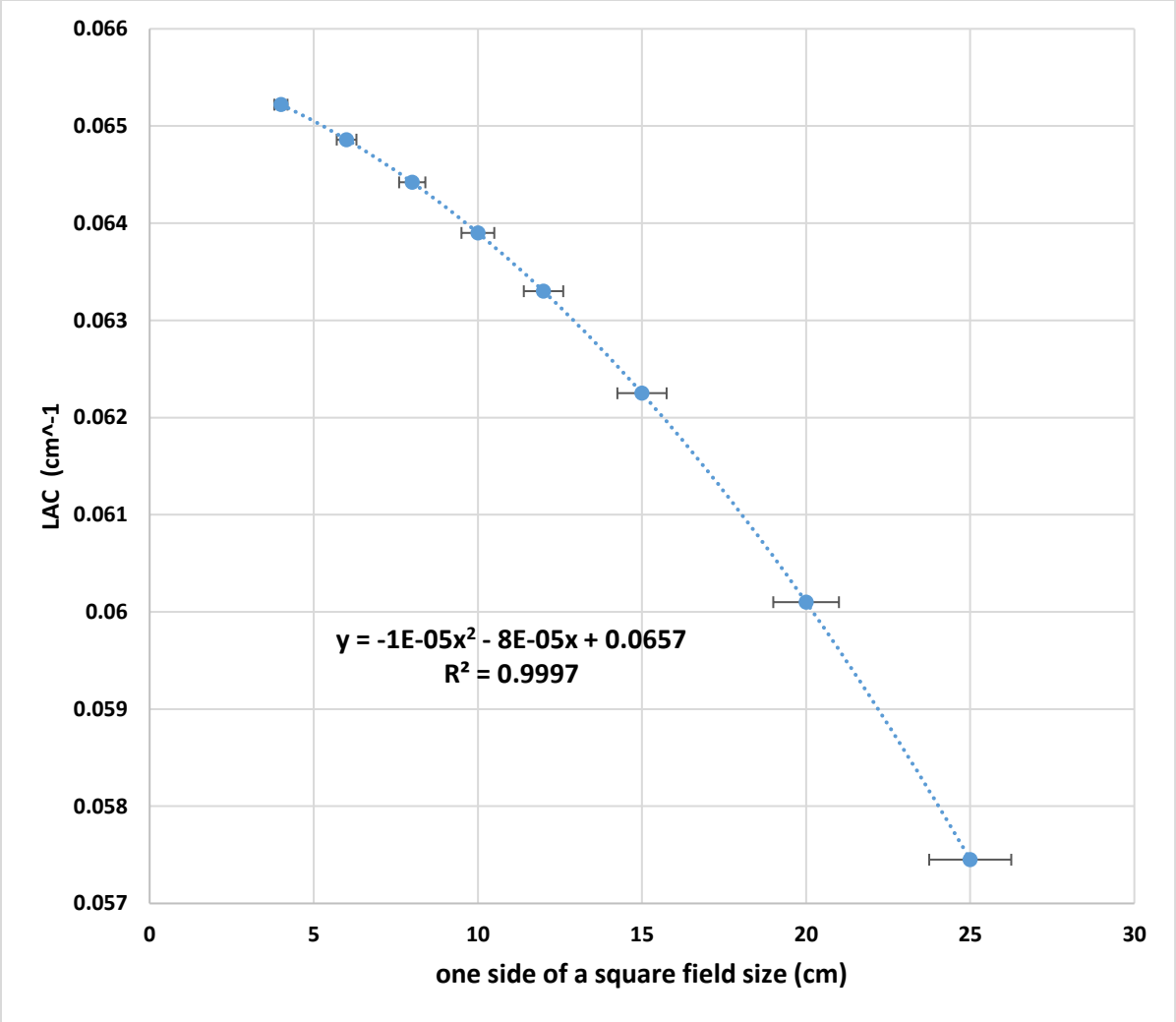

Figure 4. 2: Graph of LAC against Square field size

Although Excel produced the equation of the straight line from the data obtained, to determine the effective LAC, the field size values were substituted in place of *x* in equation 4.0 to compute the for effective LAC.

The effective LAC, μ_{eff} was used in the estimation of the primary component in the phantom material, and it defines the attenuation of the beam in the medium (phantom) with respect to field size, *x*. Table 4.2 shows the estimated effective LAC with respect to field sizes

Table 4. 2: Table of one side of a square field against Effective Linear Attenuation Coefficient

One side of a square field (cm)	Effective LAC (cm^{-1})
4	0.06522
6	0.06486
8	0.06442
10	0.0639
12	0.0633
15	0.06225
20	0.0601
25	0.05745
30	0.0543
35	0.05065

4.4.3 Total, Primary and Scattered component of PDD

Table 4. 3: Measured PDD component for various depths and field sizes

MEASURED COMPONENT OF PDD										
Depth (cm)	One side of a square field size (cm)									
	4	6	8	10	12	15	20	25	30	35
2	92.43	93.29	94.15	94.10	94.21	94.36	94.60	94.91	95.07	94.72
3	87.00	88.00	88.99	89.67	89.81	90.01	90.43	91.00	91.28	90.87
5	75.57	77.40	79.23	79.99	80.50	81.26	81.95	82.86	83.32	83.28
10	51.47	54.16	56.85	58.36	59.42	61.03	62.33	64.06	64.92	65.10
15	37.14	39.62	41.47	42.62	44.37	45.96	48.05	49.09	49.54	49.99
20	23.34	25.35	27.37	29.02	30.17	31.90	33.52	35.69	36.77	37.25
25	15.68	17.29	18.90	20.14	21.17	22.70	24.20	26.21	27.21	27.81
30	10.44	11.69	12.94	13.90	14.74	15.99	17.35	19.17	20.07	20.57

Table 4.3 above represents an extract from the percentage depth dose measurements, for various depths and field sizes, which was obtained from the Korle–Bu Teaching Hospital, Radiotherapy Center.

Table 4. 4: Calculated Primary PDD component for various depths and field sizes

CALCULATED PRIMARY COMPONENT OF PDD										
Depth (cm)	One side of a square field size(cm)									
	4	6	8	10	12	15	20	25	30	35
2	88.03	88.08	88.14	88.21	88.29	88.43	88.71	89.06	89.49	89.98
3	80.88	80.95	81.04	81.15	81.27	81.48	81.92	82.47	83.12	83.88
5	68.31	68.42	68.56	68.72	68.90	69.23	69.90	70.74	71.75	72.94
10	44.92	45.08	45.27	45.49	45.75	46.21	47.16	48.36	49.83	51.59
15	29.66	29.82	30.01	30.24	30.50	30.97	31.95	33.20	34.75	36.64
20	19.66	19.80	19.97	20.18	20.41	20.83	21.73	22.88	24.33	26.12
25	13.08	13.19	13.34	13.51	13.71	14.07	14.83	15.82	17.09	18.69
30	8.73	8.82	8.94	9.07	9.24	9.53	10.15	10.98	12.04	13.41

Table 4.4 shows the estimated primary PDD as discussed in chapter 3. The PDD_p, increases with increasing field sizes but decreases with increasing depths as observed from table 4.4 above.

The primary component of the PDD increases with increasing field size but decreases with an increase in depth as observed from table 4.4.

Table 4. 5: The Scattered PDD component for various depths and field sizes

SCATTERED COMPONENT OF PDD										
	One side of a square field size (cm)									
Depth (cm)	4	6	8	10	12	15	20	25	30	35
2	1.0499	1.0591	1.0681	1.0668	1.0670	1.0671	1.0663	1.0656	1.0624	1.0526
3	1.0757	1.0869	1.0980	1.1050	1.1050	1.1047	1.1038	1.1034	1.0981	1.0833
5	1.1063	1.1312	1.1556	1.1640	1.1682	1.1737	1.1722	1.1713	1.1612	1.1417
10	1.1458	1.2015	1.2560	1.2828	1.2989	1.3207	1.3155	1.3244	1.3028	1.2618
15	1.1720	1.2585	1.3220	1.4096	1.4546	1.4839	1.5038	1.4786	1.4255	1.3642
20	1.1867	1.2803	1.3704	1.4381	1.4778	1.5309	1.5428	1.5597	1.5113	1.4259
25	1.1987	1.3102	1.4169	1.4912	1.5440	1.6138	1.6324	1.6567	1.5923	1.4877
30	1.1961	1.3255	1.4486	1.5321	1.5958	1.6788	1.7096	1.7464	1.6667	1.5335

Table 4.5 shows the scatter PDD component for various depths and field sizes. It can be observed that the scatter function Ks increases with increasing field size and depth. As the field size is increased, the scatter function contribution to the absorbed dose also increases. Since increase in the scatter function is more at higher depths than at the depth of dmax, the PDD increases with increasing field size.

4.4.4 Equation of the scattered function Ks

Logarithm fit to the *Scattered function of the PDD component resulted in an equation*

$$y = 0.0566ln(x) + 1.0138 \ldots\ldots\ldots\ldots\ldots\ldots eqn\ 4.1$$

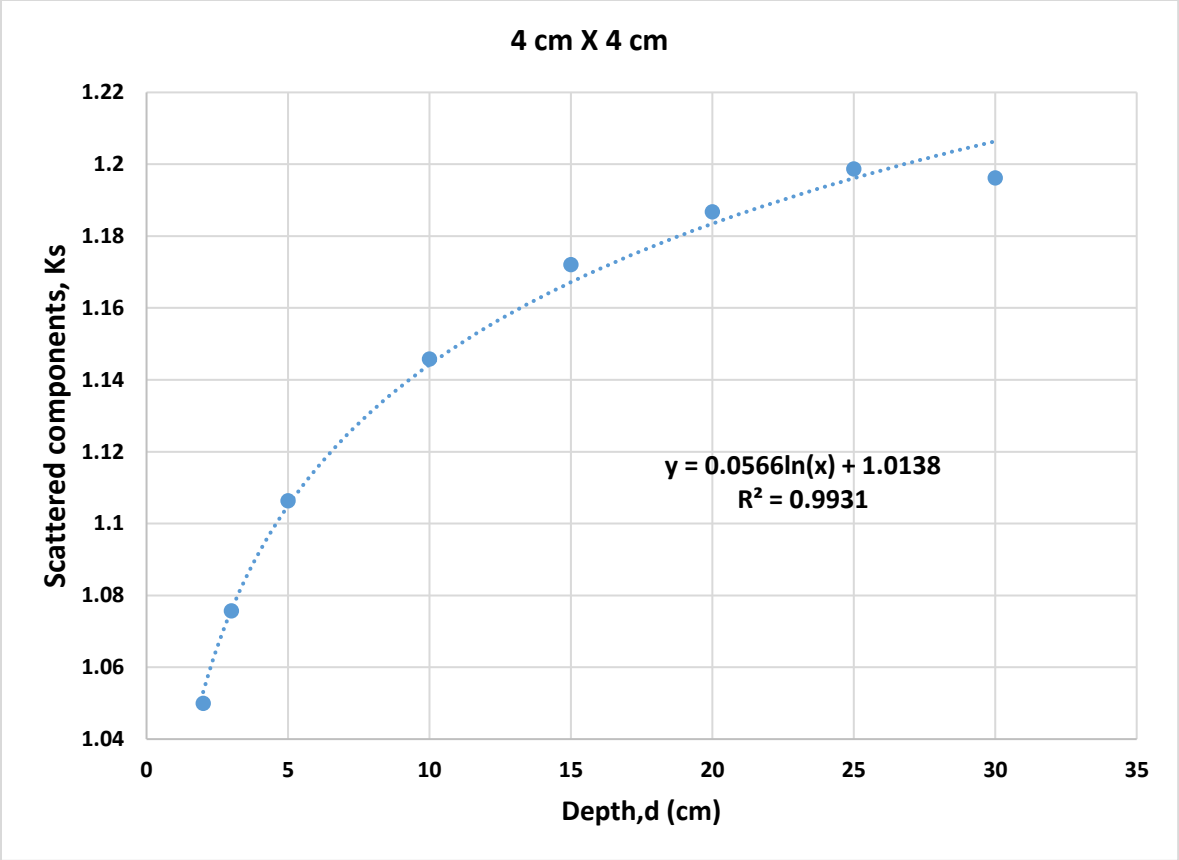

Figure 4. 3: Plot of the scattered function (Ks) and depths, d (cm)

Figure 4.3 shows K_s versus d(cm) for field size of 4 cm x4 cm. This represents the equation of the scattered function Ks as stated in equation 3.3. This implies that,

$$K_s = aln(d) + b \ldots\ldots\ldots\ldots eqn\ 4.2.$$

where K_s is the Scattered function, *'x=d'* is the depth and the constants 'a' and 'b' were determined from the plotted graph thus can be generated as shown in table 4.6 below:

Table 4. 6: Field size and the values of the constants a and b

One side of a square field size (cm)	a	b
4	0.0566	1.0139
6	0.1017	0.9775
8	0.1434	0.9438
10	0.1779	0.9105
12	0.2017	0.8844
15	0.2314	0.8503
20	0.2417	0.8369
25	0.2513	0.822
30	0.2239	0.848
35	0.1819	0.884

From the equation stated above, it can be deduced that the scatter component of the depth dose is dependent on both depth (treatment depth) and field size. This is because the constants ‘a’ and ‘b’ are dependent on field size and Ks is dependent on depth, ‘a’ and ‘b’, thus Ks is depth and field size dependent.

4.4.5 Equations for the constants 'a' and 'b'

A second order polynomial extrapolation yielded equations of 'a' to be $y = -0.0005x^2 + 0.0249x - 0.0247$ and that of 'b' to be $y = 0.0005x^2 - 0.0235x + 1.0981$ to field size with $R^2 = 0.9942$ and $R^2 = 0.9863$ respectively as shown in figure 4.4 and 4.5.

Thus the 'a' is be determined as

$$a = -0.0005r^2 + 0.0249r - 0.0247 \ldots\ldots\ldots eqn\ 4.3$$

And equation for 'b' is

$$b = 0.0005r^2 - 0.0235r + 1.0981 \ldots\ldots\ldots\ldots eqn\ 4.4$$

Both 'a' and 'b' is dependent on the field size *r*.

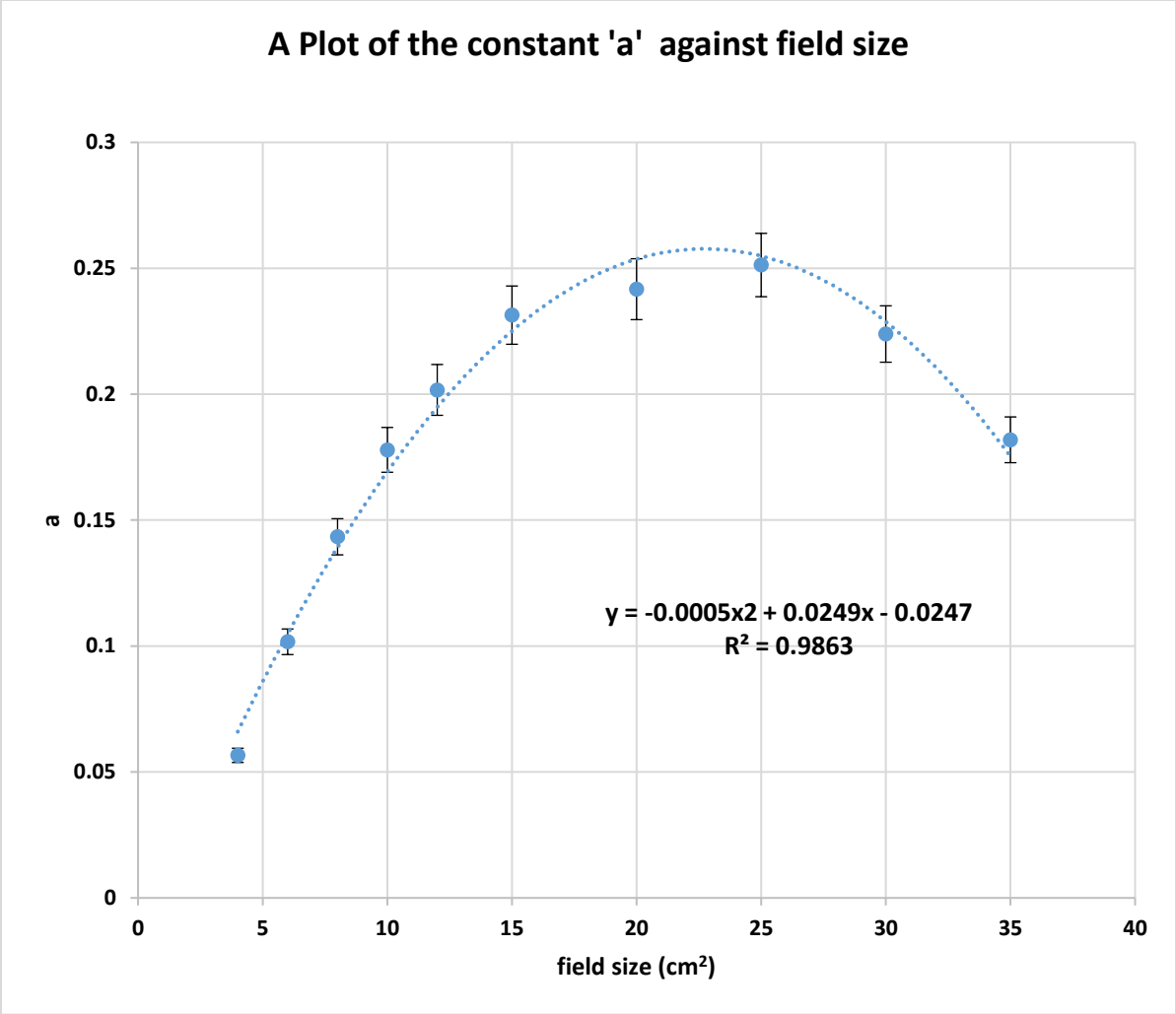

Figure 4. 4: A Plot of the constant 'a' against field size

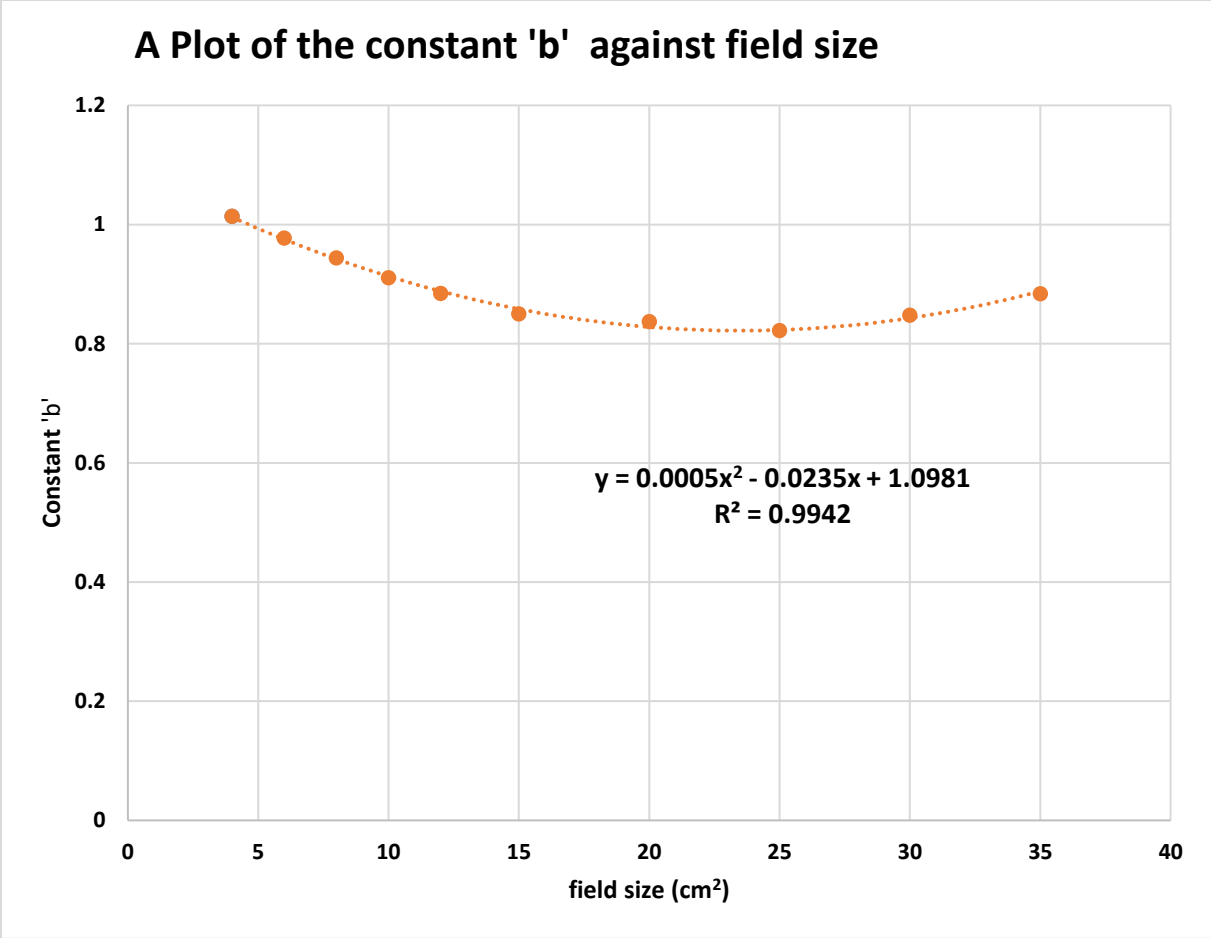

Figure 4. 5: A Plot of the constant 'b' against field size

Therefore the equation for the central axis depth dose is;

$$PDD(d, A, f, hv) = 100\left(\frac{f+d_{max}}{f+d}\right)^2 e^{-\mu_{eff}(d-d_{max})} \cdot [aln(d) + b] \ldots\ldots\ldots eqn\ 4.5.$$

where $[aln(d) + b] = K_s$, *the scattered function of the PDD component*

Table 4. 7: Shows the depth, field size and the % difference of some tested depths and field sizes

Depth *(cm)*	**field size (cm^2)**	**%Difference**
4.94	4	0.835174
5.94	4	0.827921
6.94	4	0.621066
7.94	4	1.12991
8.94	4	1.03548
9.94	4	0.906949
10.94	4	0.689377
11.94	4	0.805957
12.94	4	0.784735
13.94	4	0.811224
14.94	4	0.994657
15.94	4	0.72759
17.94	8	0.61437
18.94	8	0.66616

19.94	8	0.453424
20.94	8	1.159289
21.94	8	1.162363
22.94	8	1.140108
23.94	8	1.228116
24.94	8	1.549665
25.94	8	1.699185
26.94	8	1.254457
27.94	8	2.010412
8.94	12	3.601173
9.94	12	3.557871
10.94	12	3.239506
11.94	12	2.720847
12.94	12	2.646685
13.94	12	2.424339
14.94	12	1.956431
22.94	25	0.799147

23.94	25	0.191957
24.94	25	0.254728
20.94	25	1.824509
21.94	25	1.109849
22.94	30	1.952011
23.94	30	1.549991
24.94	30	1.225322
25.94	30	0.815949
26.94	30	0.41111
27.94	30	0.096381
28.94	30	0.420452
29.94	30	0.745728
30.94	30	0.119349
	Average	1.244794
	Minimum	0.096381
	Maximum	3.601173
	Std	0.875425

Table 4.7 shows the depth, field size and the percentage difference of tested depths and field sizes (50 field sizes). The percentage difference between the measured PDD and the calculated PDD using the proposed formula for 50 tested field sizes ranged from 0.10% to 2.01% (mean of 1.24±0.88%), which is within the 2% acceptable limit for central axis parameter constancy (PDD, TAR) as stated in the report of the TG-40. the percentage difference is expressed as the percentage of the ratio of the difference in PDD to the measured PDD.

CHAPTER FIVE

CONCLUSION AND RECOMMENDATION

5.1 CONCLUSION

A semi- empirical formula was developed and proposed for the determination of central axis depth dose of an Equinox 100 telecobalt machine. Depth doses (PDDs) calculated with the proposed formula compared to the measured depth doses (PDD data) that were obtained during commissioning of the Equinox 100 telecobalt machine was within the 2% acceptable limit for central axis parameter constancy (PDD, TAR) as stated in the report of the TG-40.

5.2 RECOMMENDATION

Based on the findings of this study and the literature reviewed, the researcher recommends the following to the various stakeholders in the Research Community and the Clinical Community in order to improve on this research work:

5.2.1 For the research community

For further studies, this research work can be done by using the LINAC. Furthermore the model obtained for the scatter function can be fined-tuned for much better accuracy in measurement and modeling can also be done in 3-Dimension. Though the output of the formula was within the acceptable limit (2%), some points deviated from the acceptable limit and this needs to be investigated in further studies.

5.2.2 For the clinical community

It is recommended that a calculation table similar to TPR or TMR tables for the variations of depth and field size with respect to the primary and scatter function Ks, be created for

dose distribution calculations done by the physicist and monthly evaluation of Ks value by the NCRNM should be done to help provide an efficient and accurate dosimetry for patient treatment. Based on the output of the proposed formula, this can for checking measured PDD.

REFERENCES

AAPM Task Group 40. See Kutcher, G.J., Coia, L., Gillin, M., Hanson, W., Leibel, S., Morton, R., Palta, J., Purdy, J., Reinstein, L., Svensson, G., Weller, M., & Wingfield, L. 1994.

Ahnesjö, A., & Ahnesj, A. (2014). Dose calculations for external photon beams in radiotherapy, (May). http://doi.org/10.1088/0031-9155/44/11/201

Ahnesjo A., (1994). "Analytic modeling of photon scatter from flattening filters in photon therapy beams," *Med. Phys*. 21:1227–35

Ahnesjö, A. (1989). Collapsed cone convolution of radiant energy for photon dose calculation in heterogeneous media. *Medical Physics*, *16*(4), 577–592. http://doi.org/10.1118/1.596360

Ahnesjo A., Andreo P., and Brahme A., (1987). "Calculation and application of point spread functions for treatment planning with high energy photon beams", *Acta Oncologica* 26:49–56 2:275–292 (1984).

Bjarngard B. E. and Petti P. L., (1988). "Description of the scatter component in photonbeam data," *Phys. Med. Biol.* 33:21–32.

Booz J., Ebert H. G., Eickel R., and Waker A. (eds.) (1974). (Luxembourg: Commission of the European Communities), pp. 677–93

Bortfeld T., Schlegel W., and Rhein B., (1993). "Decomposition of pencil beam kernels for fast dose calculations in three-dimensional treatment planning," *Med. Phys.* 20:311–18

Brahme Anders and Svensson Hans (1988). "Accuracy requirement and quality assurance of external beam therapy with photons and electrons," *Acta Radiol. Oncol. Suppl.1*

Buzdar SA, Rao MA, Nazir A. An analysis of depth dose characteristics of phtons in water. J Ayub Med Coll 2009;21(4):4,41–5.

Chaikh A, Khamphan C, Kumar T, Garcia R, Balosso J. (2016) What should we know about photon dose calculation algorithms used for radiotherapy? Their impact on dose distribution and medical decisions based on TCP/NTCP. Int J Cancer Ther Oncol.; 4(4):4418. DOI: 10.14319/ijcto.44.18

Cunningham J. R. and Beaudoin L., (1973). "Calculations for tissue inhomogeneities with experimental verification," *Proceedings of the XIII International Congress of Radiology*, Madrid, pp. 653–7

Difilippo F C 1998 Forward and adjoint methods for radiotherapy planning Med. Phys. 25 1702–10

Dunscombe, P., Johnson, H., Arsenault, C., Bissonnette, J-P., Johnson, H., Mawko, G., & Seuntjens, J .2007. Development of quality control standards for radiation therapy equipment in Canada. *Journal of Applied Clinical Medical Physics,* Vol.8,1;108-118.

Dutreix A. and Bridier A., (1985). "Dosimetry for External Beams of Photon and Electron Radiation" (Chapter 3) in *The Dosimetry of Ionizing Radiation,*" Kenneth R. Kase, Bengt Björngard, and Frank Attix (eds.), (San Diego: Academic Press Inc., Harcourt Brace Jovanovitch) V.1, pp. 163–228

Dutreix A., Bjarngard B. E., Bridier A., Mijnheer B., Shaw J. E., and Svensson H., (1997). "Monitor Unit Calculation For High Energy Photon Beams," in *Physics for Clinical Radiotherapy Booklet No. 3*, European Society for Therapeutic Radiology and Oncology (ESTRO), ed. Garant Publishers N.V.

Dutreix A., (1966). "When and how can we improve precision in radiotherapy?" *Radiother. Oncol.*

Dutreix J. and Bernard M., "Dosimetry at interfaces for high energy X and gamma rays," *Br. J. Radiol.* 39:205–210

Dutreix J., Dutreix A., and Tubiana M., (1965). "Electronic equilibrium and transition stages." *Phys. Med. Biol.* 10:177–190

Fano U., (1954). "Note on the Bragg-Gray cavity principle for measuring energy dissipation," *Radiat. Res.* 1:237–40

Fogarty, G.B., Hornby, C., Ferguson, H.M., & Peters, L.J. 2001. Quality assurance in radiation oncology unit: The chart round experience. Australasian Radiology, 45;189-194.

Gibbons, J. P., Antolak, J. A., Followill, D. S., Klein, E. E., & Reid, M. (2014). Monitor unit calculations for external photon and electron beams : Report of the AAPM Therapy Physics Committee Task Group No . 71, *41*(71), 1–34.

Harder D., "Fano's theorem and the multiple scattering correction," *Fourth Symposium On Microdosimetry* (Verbania –Pallanza, Italy)

Hudej, R. (2008).TELERADIOTHERAPY DOSE CALUCULATION Aljaˇ sa Jenko,

Holt J G, Laughlin J S and Moroney J P 1970 The extension of the concept of tissue-air ratios (TAR) to high-energy x-ray beams Radiology 96 437–46

IAEA, (1987). Absorbed Dose Determination in Photon and electron Beams. An International Code of Practice, IAEA Technical Report Series No. 277 (Vienna: International Atomic Energy Agency)

IAEA, (2000). Absorbed Dose Determination in External Beam Radiotherapy: An International Code of Practice for Dosimetry Based on Standards of Absorbed Dose to Water (International Atomic Energy Agency, Vienna, 2000).

International Atomic Energy Agency. TRS-398, Absorbed dose determination in external beam radiotherapy: an international code of practice for dosimetry based on standards of absorbed dose to water. Vienna: IAEA; 2000.

IAEA, (1997). Quality assurance in radiotherapy. TECDOC-989. Vienna: IAEA; 1997.

ICRU Report No. 24, (1976). "Determination of Absorbed Dose in a Patient Irradiated by Beams of X or Gamma Rays in Radiotherapy Procedures," (Washington, DC: International Commission on Radiation Units and Measurements).

ICRU Report No. 42,1987 Use of computers in external beam radiotherapy procedures with high-energy photons and electrons ICRU Publication 42 (Bethesda, MD: International Commission on Radiation Units and Measurements.

ICRU Report No. 42, (1973). Measurement of absorbed dose in a phantom irradiated by a single beam of x or gamma rays ICRU Publication 23 (Bethesda, MA: International Commission on Radiation Units and Measurements)

ICRU 1963 Clinical dosimetry handbook 87 ICRU Publication 10d (Washington, DC: National Bureau of Standards).

International Commission on Radiation Units and Measurements. Prescribing, recording and reporting photon beam therapy. Report 50, USA: ICRU; 1993.

Karlsson M, Ahnesjö A, Nyholm T, Georg D and Olofsson J. (2010). Independent Dose Calculations Concepts and Models.

Johns H. E. and Cunningham J. R., (1983). *The Physics of Radiology*, (Springfield, IL: C.C. Thomas)

Johns H. E., Darby E. K., Haslam R. N., Katz L., and Harrington E. L., (1949). "Depth dose data and isodose distributions for radiation from a 22 MeV betatron," *Am. J. Roentgenol.* 62:257 68

Karzmark C J, Deubert A and Loevinger R 1965 Letter to Editor: tissue-phantom ratios—an aid to treatment planning Br. J. Radiol. 38 158–9

Khan FM, editor. The physics of radiation therapy 4 th Edition, USA: Lippincott Williams & Wilkins; 2010.p. 176– 8.

Memon, S. A., Cheema, A. A., Laghari, N. A., & Mangi, F. H. (2014). Dose measurement of cobalt-60 radiotherapy beams in treatment fields DOSE MEASUREMENT OF COBALT-60 RADIOTHERAPY BEAMS IN TREATMENT FIELDS, (December).

Memon, S. A., Laghari, N. A., Mangi, F. H., Jafri, M. A., & Raza, M. (2017). Dosimetric Conformity of Cobalt-60 (Co 60) Beams Dosimetric Conformity of Cobalt-60 (Co

60) Beams, *60*(July).

Mohan R.and Chui C.-S., (1985). "Validity of the concept of separating primary and scatter dose," *Med. Phys.* 12:726–30.

Nyholm T, Olofsson J, Ahnesjö A and Karlsson M 2006c Photon pencil kernel parameterization based on beam quality index Radiother Oncol 78 347-51

O'Connor J. E., (1957). "The variation of scattered x-rays with density in an irradiated body," *Phys. Med. Biol.* 1:352–69.

O'Connor J E and Malone D E 1989 A cobalt-60 primary dose spread array derived from measurements Phys. Med. Biol. 34 1029–42

Of, D., Timer, T., On, E., Boakye, N. K., In, L., Fulfillment, Award, T. H. E. (2016). University of Ghana http://ugspace.ug.edu.gh, (10508448).

Papanikolaou N., Erb J., Gehring M., Sanders C., (1997). "Commissioning and Acceptance Testing of a Convolution based 3D RTP System," in *Medical & Biological Engineering & Computing*, V. 35, Suppl. Part 2, p. 994, Nice 1997, World Congress on Medical Physics 994, Nice

Pacyniak J. Analytic derivation of central axis percent depth dose calculations in transition zones with loss of electronic equilibrium. Int J Cancer Ther Oncol. 2016; 4(3):436. DOI: 10.14319/ijcto.43.6

Papanikolaou N.and Heintz B., (1996). "Speed and accuracy considerations for convolution algorithms in 3D treatment planning," *Med. Phys.* 23.

Papanikolaou N., Mackie T. R., and Gehring M., (1995). "A Convolution Based Algorithm for Dose Computation in Radiation Therapy," in *Proceedings of the Roentgen Centennial International Congress*, Wurzburg-Germany.

Papanikolaou N.and Mackie T. R., (1995). "Extension of the convolution/superposition based algorithms to include atomic number effects," *Med. Phys.* 22:977

Papanikolaou N.and Mackie T. R., (1994). "Separation of photon beam output factor into its phantom and machine generated components using a convolution code," *Med. Phys.* 21:877–878

Papanikolaou N.and Mackie T. R., (1994). "The extended phantom concept: modeling the treatment machine modifiers and portal imaging dosimetry system using a convolution code," *Med. Phys.* 21:877

Papanikolaou N., Mackie T. R., Meger-Wells C., Gehring M., and Reckwerdt P., (1993). "Investigation of the convolution method for polyenergetic spectra," *Med. Phys*. 20:1327–1336.

Peiffert, D., Simon, J.M., and Eschwege, F. 2007. Epinal radiotherapy accident: passed, present, future. Cancer Radiother, 11(6-7); 309-12.

Reddy, K. S. (1899). Choice Of A Teletherapy Unit : Cobalt 60 Unit Vs Linear Accelerator, 79–87.

Rock, L., Battista, J. J., Regional, L., Centre, C., Boyer, A. L., Kappas, C., … Mackie, T. R. (n.d.). *Tissue Inhomogeneity Corrections For Megavoltage Photon Beams*.

Sharpe M. B., Jaffray D. A., Battista J. J., Munro P., (1995). "Extrafocal radiation: a unified approach to the prediction of beam penumbra and output factors for megavoltage x-ray beams," *Med. Phys.* 22:2065–2074.

Thoraeus, R. (2017). Chapter III . Standard Measurements of the Cobalt 60 Gamma Radiation, *6926*(October). http://doi.org/10.3109/00016925909173793

Thwaites, D., Scalliet, P. Leer, J.W., Overgaard, J. 1995. Quality assurance in radiotherapy. European Society for Therapeutic Radiology and Oncology Advisory Report to the Commission of the European Union for the 'Europe Against Cancer Programme'. Radiother Oncol, 35(1); 61-73.

Venselaar J., Welleweerd H., and Mijnheer B., (2001). "Tolerances for the accuracy of photon beam dose calculations of treatment planning systems," *Radiother. Oncol.* 60:191–201

Woo M. K., Cunningham J. R., and Jeziorenski J. J., (1990). "Extending the concept of primary and scatter separation to the condition of electronic disequilibrium," *Med. Phys*. 17:588–595

Woo M. K. and Cunningham J. R., (1990). "The validity of the density scaling method in primary electron transport for photon and electron beams," *Med. Phys*. 17:187–194

Xhafa1 B., Mulaj T., Hodolli1 G., Nafezi G. Dose Distribution of Photon Beam by Siemens Linear Accelerator. Faculty of Medicine, University of Prishtina, Prishtina, Kosovo. Department of Physical Engineering, Polytechnic University of Tirana, Tirana, Albania. Department of Physics, Faculty of Natural Science,

University of Prishtina, Prishtina, Kosovo

APPENDICES

Appendix A – I show the Tables of the ion chamber reading at 60 seconds responds and it correspondent corrected readings.

Appendix A: table 1

2x2						
depth	readings	T_i	T_f	Av. Temp	Cor. Read	Ln Read
0	2.684	26.2	26.3	26.25	2.745966	1.010133
2	2.35	26.3	26.3	26.3	2.404656	0.877407
4	2.042	26.3	26.2	26.25	2.089144	0.736754
6	1.789	26.2	26.2	26.2	1.829997	0.604314
8	1.629	26.3	26.3	26.3	1.666887	0.510958
10	1.427	26.3	26.2	26.25	1.459945	0.378399
12	1.24	26.2	26.2	26.2	1.268416	0.237769

Appendix B: table 2

4x4						
depth	readings	T_i	T_f	Av. Temp	Cor. Read	Ln Read.
0	3.233	26.2	26.2	26.2	3.307088	1.196068
2	2.818	26.2	26.2	26.2	2.882578	1.058685
4	2.476	26.3	26.3	26.3	2.533587	0.929636
6	2.169	26.2	26.3	26.25	2.219076	0.797091
8	1.917	26.2	26.2	26.2	1.960931	0.673419
10	1.676	26.2	26.3	26.25	1.714694	0.539235
12	1.475	26.2	26.2	26.2	1.508802	0.411316

Appendix C: table 3

6x6						
depth	readings	T_i	T_f	Av. Temp	Cor. Read	Ln Read
0	3.28	26.2	26.2	26.2	3.355165	1.210501
2	2.863	26.2	26.2	26.2	2.928609	1.074528
4	2.517	26.3	26.3	26.3	2.57554	0.946059
6	2.204	26.3	26.3	26.3	2.255261	0.813266
8	1.948	26.2	26.2	26.2	1.992641	0.689461
10	1.706	26.3	26.3	26.3	1.745678	0.557143
12	1.502	26.2	26.2	26.2	1.53642	0.429455

Appendix D: table 4

8x8						
depth	readings	T_i	T_f	Av. Temp	Cor. Read	Ln Read
0	3.325	26.2	26.2	26.2	3.401197	1.224127
2	2.904	26.2	26.3	26.25	2.971045	1.088914
4	2.555	26.3	26.3	26.3	2.614424	0.961044
6	2.239	26.3	26.4	26.35	2.291457	0.829188
8	1.981	26.4	26.3	26.35	2.027413	0.70676
10	1.737	26.3	26.3	26.3	1.777399	0.575151
12	1.53	26.3	26.2	26.25	1.565323	0.448092

Appendix E: table 5

10x10						
depth	readings	T_i	T_f	Av. Temp	Cor. Read	Ln Read
0	3.369	26.3	26.2	26.25	3.446781	1.237441
2	2.942	26.3	26.3	26.3	3.010425	1.102081
4	2.592	26.3	26.3	26.3	2.652285	0.975421
6	2.276	26.4	26.4	26.4	2.329713	0.845745
8	2.015	26.3	26.4	26.35	2.062209	0.723778
10	1.769	26.3	26.3	26.3	1.810143	0.593406
12	1.559	26.3	26.3	26.3	1.595259	0.467036

Appendix F: table 6

12x12						
depth	readings	T_i	T_f	Av. Temp	Cor. Read	Ln Read
0	3.407	26.3	26.3	26.3	3.48624	1.248824
2	2.981	26.3	26.3	26.3	3.050332	1.11525
4	2.631	26.2	26.3	26.25	2.691742	0.990189
6	2.311	26.4	26.5	26.45	2.365934	0.861173
8	2.049	26.3	26.3	26.3	2.096656	0.740344
10	1.801	26.3	26.4	26.35	1.843195	0.611501
12	1.59	26.2	26.3	26.25	1.626709	0.486559

Appendix G: table 7

15x15						
depth	readings	T_i	T_f	Av. Temp	Cor. Read	Ln Read
0	3.458	26.3	26.3	26.3	3.538426	1.263682
2	3.036	26.3	26.3	26.3	3.106611	1.133533
4	2.683	26.2	26.2	26.2	2.744484	1.009593
6	2.364	26.5	26.4	26.45	2.420194	0.883848
8	2.102	26.2	26.3	26.25	2.150529	0.765714
10	1.851	26.4	26.3	26.35	1.894367	0.638885
12	1.636	26.2	26.2	26.2	1.673491	0.514912

Appendix H: table 8

20x20						
depth	readings	T_i	T_f	Av. Temp	Cor. Read	Ln Read
0	3.53	26.4	26.3	26.35	3.612704	1.284456
2	3.113	26.3	26.3	26.3	3.185402	1.158579
4	2.767	26.2	26.2	26.2	2.830409	1.040421
6	2.445	26.4	26.4	26.4	2.502701	0.917371
8	2.186	26.2	26.2	26.2	2.236095	0.804731
10	1.932	26.3	26.3	26.3	1.976934	0.681547
12	1.714	26.3	26.2	26.25	1.753571	0.561654

Appendix I: table 9

25x25						
depth	readings	T_i	T_f	Av. Temp	Cor. Read	Ln Read
0	3.552	26.2	26.4	26.3	3.634612	1.290502
2	3.176	26.3	26.2	26.25	3.249325	1.178447
4	2.839	26.2	26.2	26.2	2.904059	1.06611
6	2.522	26.4	26.4	26.4	2.581518	0.948378
8	2.261	26.4	26.2	26.3	2.313586	0.838799
10	2.008	26.3	26.2	26.25	2.054359	0.719964
12	1.788	26.2	26.3	26.25	1.82928	0.603922

Appendix J

Table 9: A table of one side of a square field against Linear Attenuation Coefficient (cm^{-1}) of cobalt 60 in water (H_2O).

One side of a square field (cm^2)	Linear Attenuation coefficient (cm^{-1})
2	0.0632
4	0.0652
6	0.0649
8	0.0645
10	0.0639
12	0.0633
15	0.0621
20	0.06
25	0.0572

Appendix K

Table 10: Shows a table of one side of a square field against Effective Linear Attenuation Coefficient

One side of a square field (cm^2)	LAC effective (cm^{-1})
4	0.06522
6	0.06486
8	0.06442
10	0.0639
12	0.0633
15	0.06225
20	0.0601
25	0.05745
30	0.0543
35	0.05065

Appendix L

Table 11: Shows the measured PDD component for various depths and field sizes

depth/ field size	4	6	8	10	12	15	20	25	30	35	40	43
-0.06	65.64	67.505	69.37	71.04	72.64	75.04	79.29	84.96	87.79	90.57	93.34	94.08
0.94	98.29	98.41	98.53	98.52	98.37	98.15	98.29	98.48	98.58	98.11	97.64	97.16
1.94	92.75	93.605	94.46	94.37	94.47	94.62	94.85	95.15	95.3	94.95	94.6	93.71
2.94	87.36	88.315	89.27	89.95	90.08	90.27	90.68	91.23	91.51	91.09	90.67	90.6
3.94	81.42	83	84.58	85.28	85.55	85.96	86.52	87.27	87.64	87.41	87.17	86.68
4.94	75.9	77.71	79.52	80.26	80.76	81.51	82.19	83.09	83.54	83.52	83.49	82.7
5.94	70.45	72.565	74.68	75.78	76.40	77.32	78.17	79.31	79.88	79.65	79.41	79.16
6.94	65.43	67.71	69.99	71.16	71.95	73.14	74.04	75.24	75.84	75.88	75.91	75.58
7.94	60.28	62.865	65.45	66.91	67.69	68.86	70.03	71.58	72.36	72.28	72.2	72.01
8.94	55.83	58.35	60.87	62.74	63.68	65.1	66.22	67.71	68.45	68.69	68.93	68.39
9.94	51.7	54.395	57.09	58.58	59.65	61.25	62.54	64.27	65.13	65.31	65.48	65.38
10.94	47.9	50.52	53.14	54.85	55.93	57.55	58.92	60.75	61.67	61.92	62.16	61.82
11.94	44.22	46.87	49.52	51.39	52.48	54.12	55.54	57.44	58.39	58.62	58.84	58.75
12.94	40.87	43.505	46.14	47.73	48.99	50.87	52.31	54.22	55.18	55.57	55.95	55.59
13.94	37.75	40.34	42.93	44.46	45.75	47.69	49.19	51.18	52.18	52.53	52.88	52.85
14.94	34.81	37.295	39.78	41.65	42.81	44.54	46.11	48.20	49.25	49.70	50.15	49.98
15.94	32.24	34.545	36.85	38.6	39.96	41.99	43.54	45.61	46.64	47.00	47.36	47.51
16.94	29.83	32.11	34.39	35.9	37.18	39.11	40.74	42.92	44.01	44.46	44.91	44.9
17.94	27.59	29.81	32.03	33.62	34.78	36.53	38.22	40.47	41.6	41.99	42.38	42.46
18.94	25.45	27.58	29.71	31.16	32.42	34.32	35.89	37.99	39.04	39.58	40.11	40.14
19.94	23.44	25.46	27.48	29.14	30.29	32.02	33.65	35.82	36.9	37.37	37.84	38.19
20.94	21.69	23.67	25.65	27.06	28.22	29.96	31.55	33.67	34.73	35.36	35.99	35.85
21.94	20.02	21.895	23.77	25.24	26.34	28	29.60	31.73	32.79	33.35	33.91	33.96
22.94	18.61	20.315	22.02	23.47	24.50	26.05	27.64	29.77	30.83	31.33	31.82	32.03
23.94	17.06	18.74	20.42	21.73	22.81	24.43	25.96	28.01	29.03	29.61	30.19	30.33
24.94	15.75	17.365	18.98	20.23	21.25	22.79	24.30	26.31	27.31	27.90	28.49	28.51
25.94	14.54	16.075	17.61	18.8	19.79	21.27	22.75	24.72	25.71	26.32	26.93	26.86
26.94	13.35	14.795	16.24	17.47	18.43	19.87	21.31	23.24	24.2	24.83	25.46	25.34
27.94	12.35	13.755	15.16	16.3	17.20	18.55	19.97	21.86	22.8	23.35	23.89	23.86
28.94	11.52	12.865	14.21	15.17	16.01	17.28	18.67	20.52	21.44	21.91	22.37	22.55
29.94	10.48	11.74	13	13.96	14.80	16.06	17.43	19.25	20.16	20.65	21.14	21.22
30.94	9.8	10.935	12.07	13	13.78	14.94	16.20	17.89	18.73	19.32	19.9	19.94

Appendix M

Table 12: Shows the estimated Primary PDD component for various depths and field sizes

Estimated Primary component of PDD										
Depth (cm)	One side of a square field size (cm)									
	4	6	8	10	12	15	20	25	30	35
2	88.03	88.08	88.14	88.21	88.29	88.43	88.71	89.06	89.49	89.98
3	80.88	80.95	81.04	81.15	81.27	81.48	81.92	82.47	83.12	83.88
5	68.31	68.42	68.56	68.72	68.90	69.23	69.90	70.74	71.75	72.94
10	44.92	45.08	45.27	45.49	45.75	46.21	47.16	48.36	49.83	51.59
15	29.66	29.82	30.01	30.24	30.50	30.97	31.95	33.20	34.75	36.64
20	19.66	19.80	19.97	20.18	20.41	20.83	21.73	22.88	24.33	26.12
25	13.08	13.19	13.34	13.51	13.71	14.07	14.83	15.82	17.09	18.69
30	8.73	8.82	8.94	9.07	9.24	9.53	10.15	10.98	12.04	13.41

Appendix N: table 13

Shows the Scattered PDD component for various depths and field sizes

SCATTERED COMPONENT OF PDD										
Depth (cm)	One side of a square field size (cm)									
	4	6	8	10	12	15	20	25	30	35
2	1.0499	1.0591	1.0681	1.0668	1.0670	1.0670	1.0663	1.0656	1.0624	1.0526
3	1.0757	1.0869	1.0980	1.1050	1.1050	1.1046	1.1038	1.1034	1.0981	1.0833
5	1.1063	1.1312	1.1556	1.1640	1.1682	1.1737	1.1722	1.1713	1.1612	1.1417
10	1.1458	1.2015	1.2560	1.2828	1.2989	1.3207	1.3215	1.3244	1.3028	1.2618
15	1.1720	1.2585	1.3220	1.4096	1.4546	1.4839	1.5038	1.4786	1.4255	1.3642
20	1.1867	1.2803	1.3704	1.4381	1.4778	1.5309	1.5428	1.5597	1.5113	1.4259
25	1.1987	1.3102	1.4169	1.4912	1.5440	1.6137	1.6324	1.6567	1.5923	1.4877
30	1.1961	1.3255	1.4486	1.5321	1.5958	1.6788	1.7096	1.7464	1.6667	1.5335

APPENDIX O

Table 14: Shows Field size and the values of the constants a and b of the Scattered function

field size (cm^2)	a	B
4	0.0566	1.0139
6	0.1017	0.9775
8	0.1434	0.9438
10	0.1779	0.9105
12	0.2017	0.8844
15	0.2314	0.8503
20	0.2417	0.8369
25	0.2513	0.8220
30	0.2239	0.8480
35	0.1819	0.8840

Appendix P: Figure 1

Shows the corrected readings versus one side of a square field size for 4 cm x 4 cm,

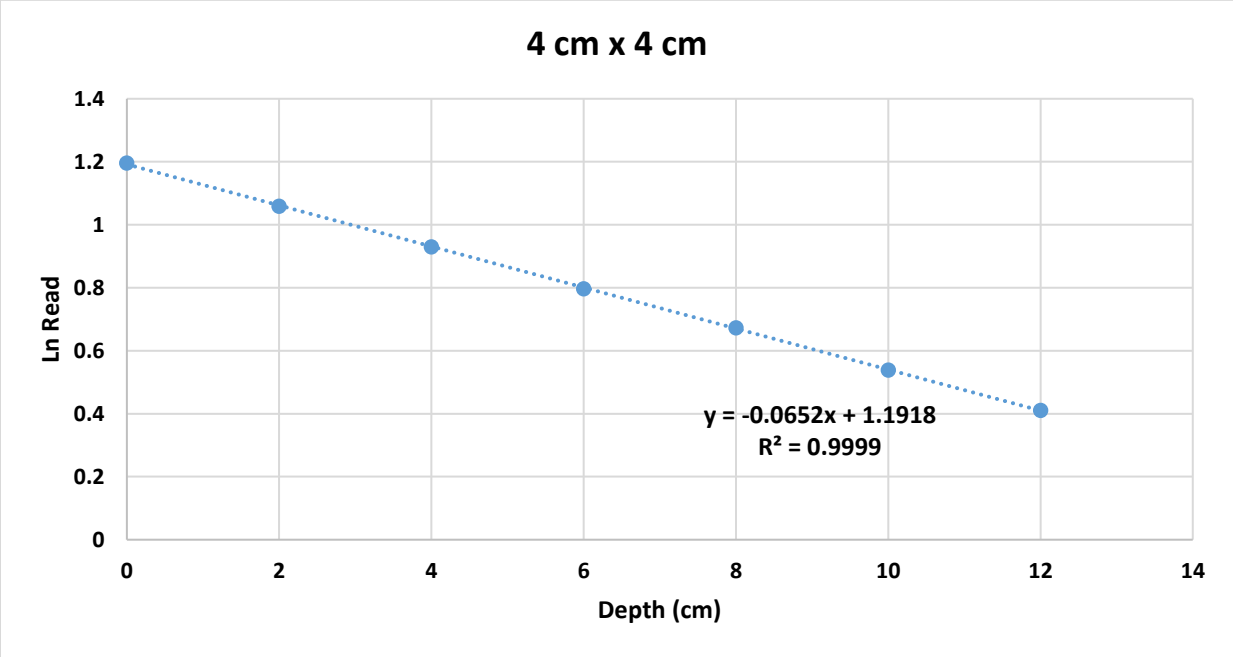

Appendix P: Figure 2

Shows the corrected readings versus one side of a square field size for 8 cm x 8 cm

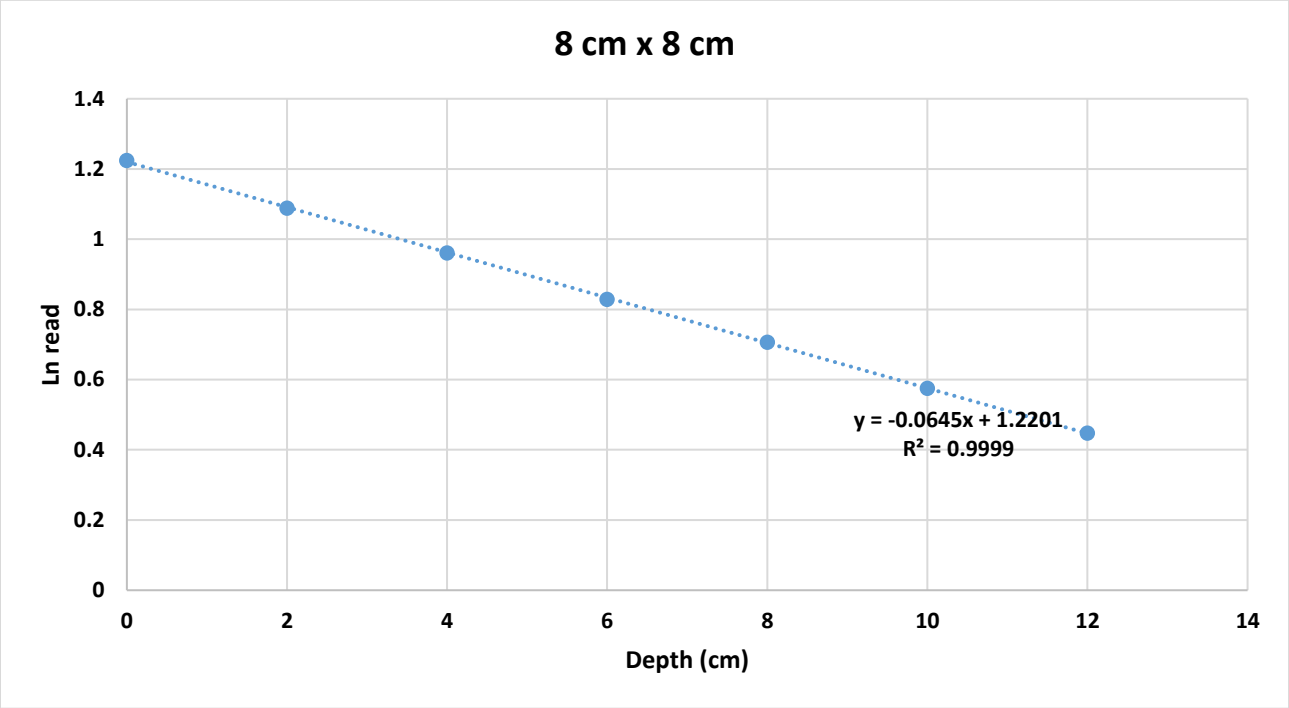

Appendix Q: Figure 3

Shows the corrected readings versus one side of a square field size for 12cm x 12cm

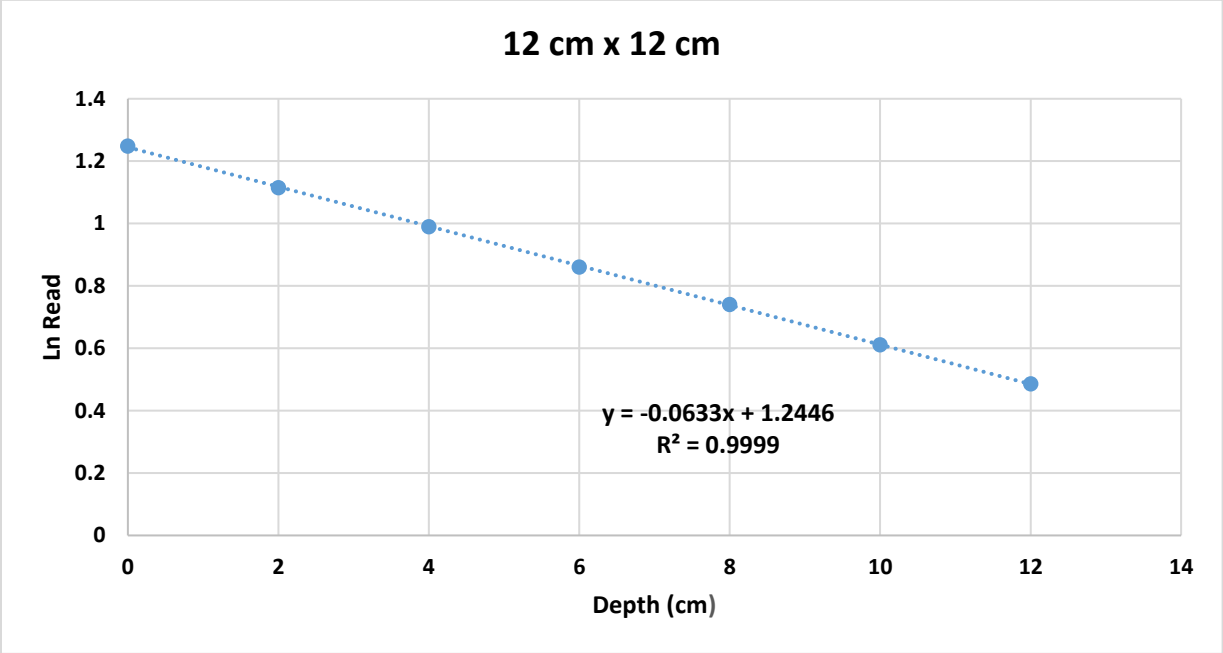

Appendix R: Figure 4

Shows the corrected readings versus one side of a square field size for 25 cm x 25 cm

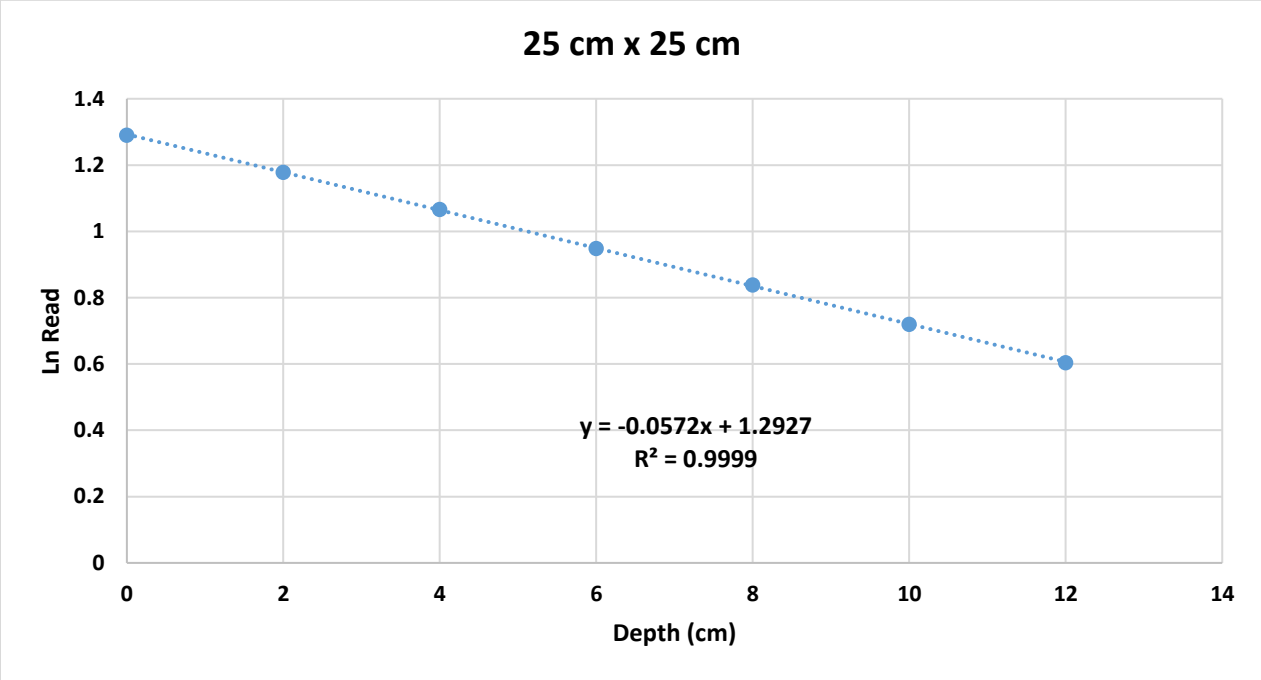

Appendix S: Figure 5

Shows the linear attenuation coefficient versus one side of a square field size for 4 cm x 4 cm

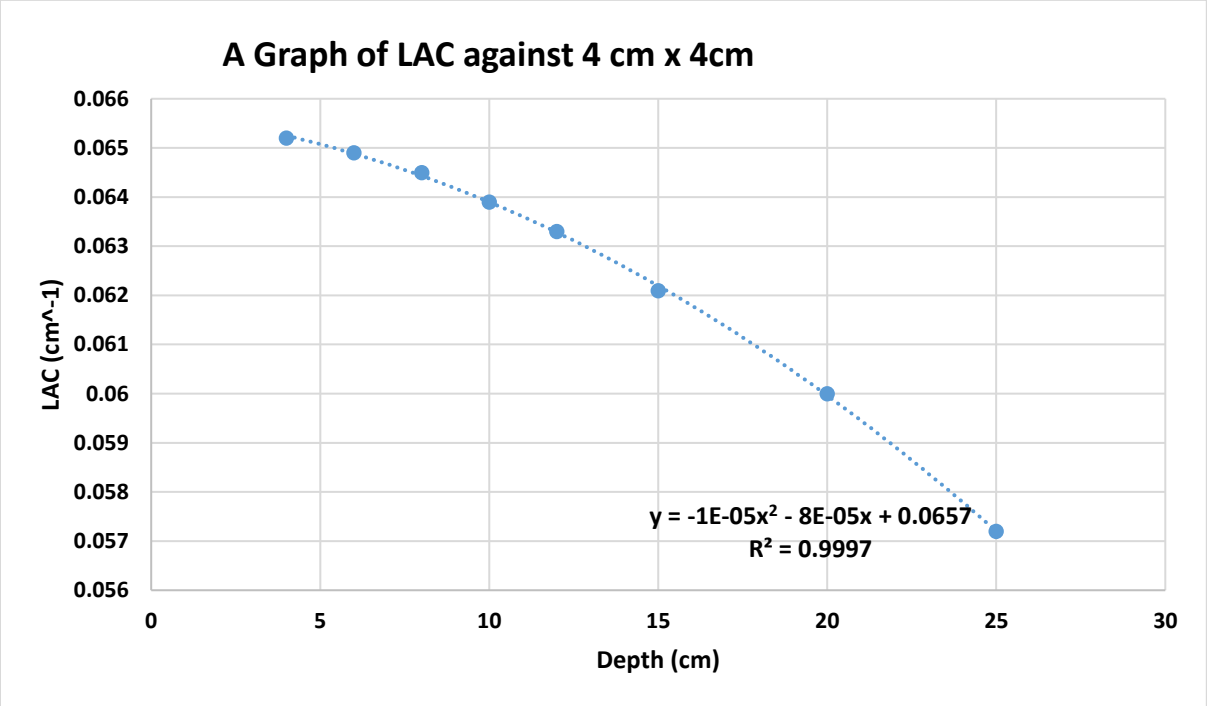

Appendix T: Figure 6

Shows the linear attenuation coefficient versus one side of a square field size for 6 cm x 6 cm

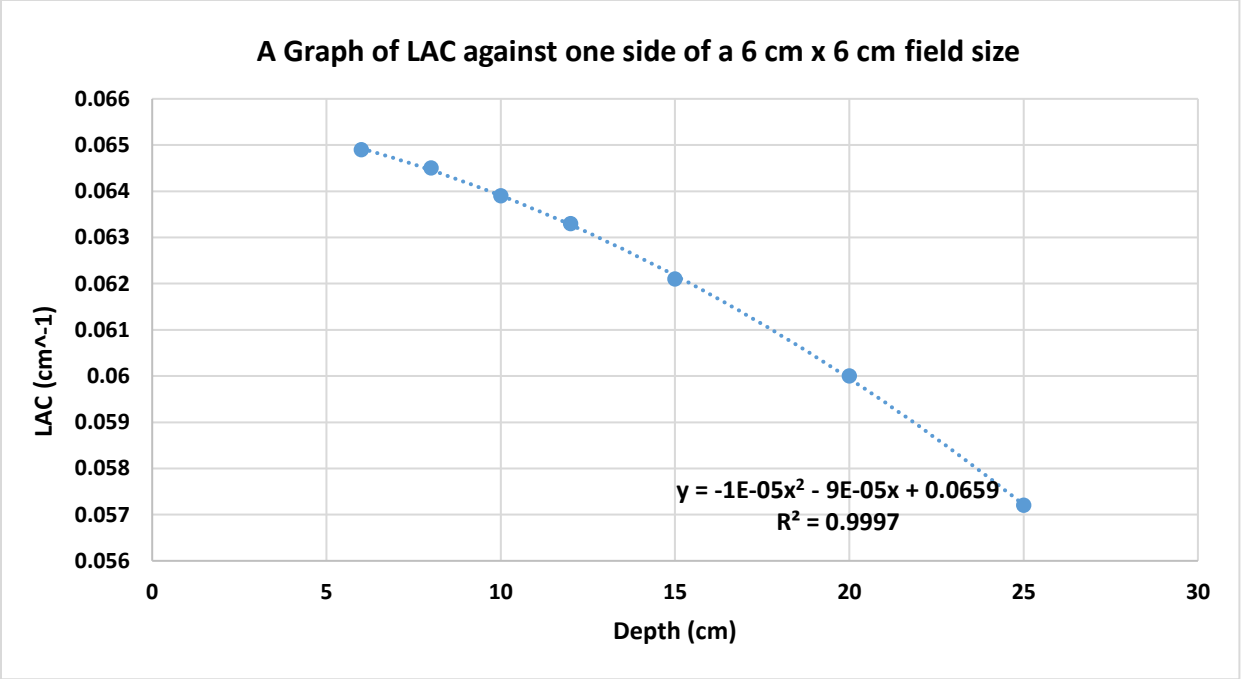

Appendix U: Figure 7

Plot of the scattered function (Ks) and depths, d (cm)

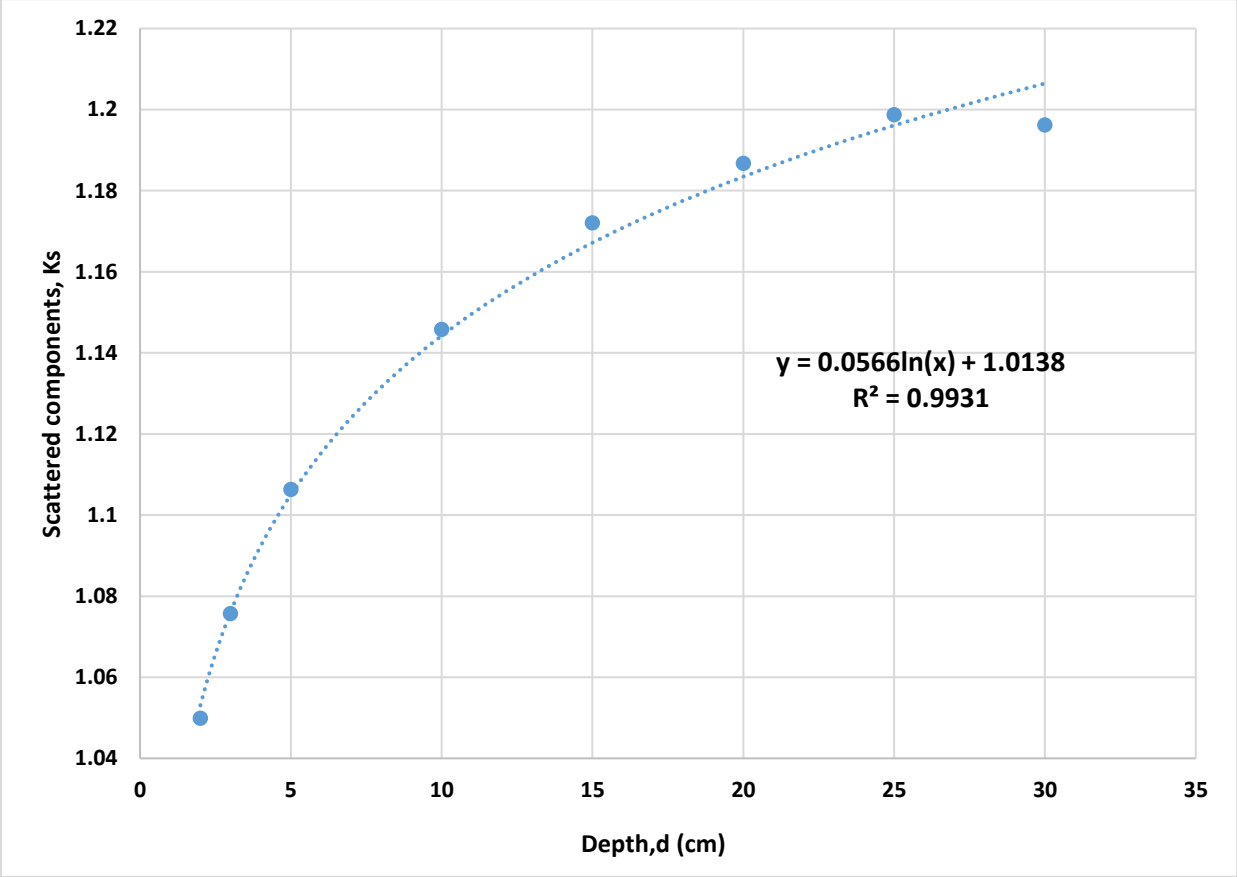

Appendix V: Figure 8

A Plot of the constant 'a' against field size

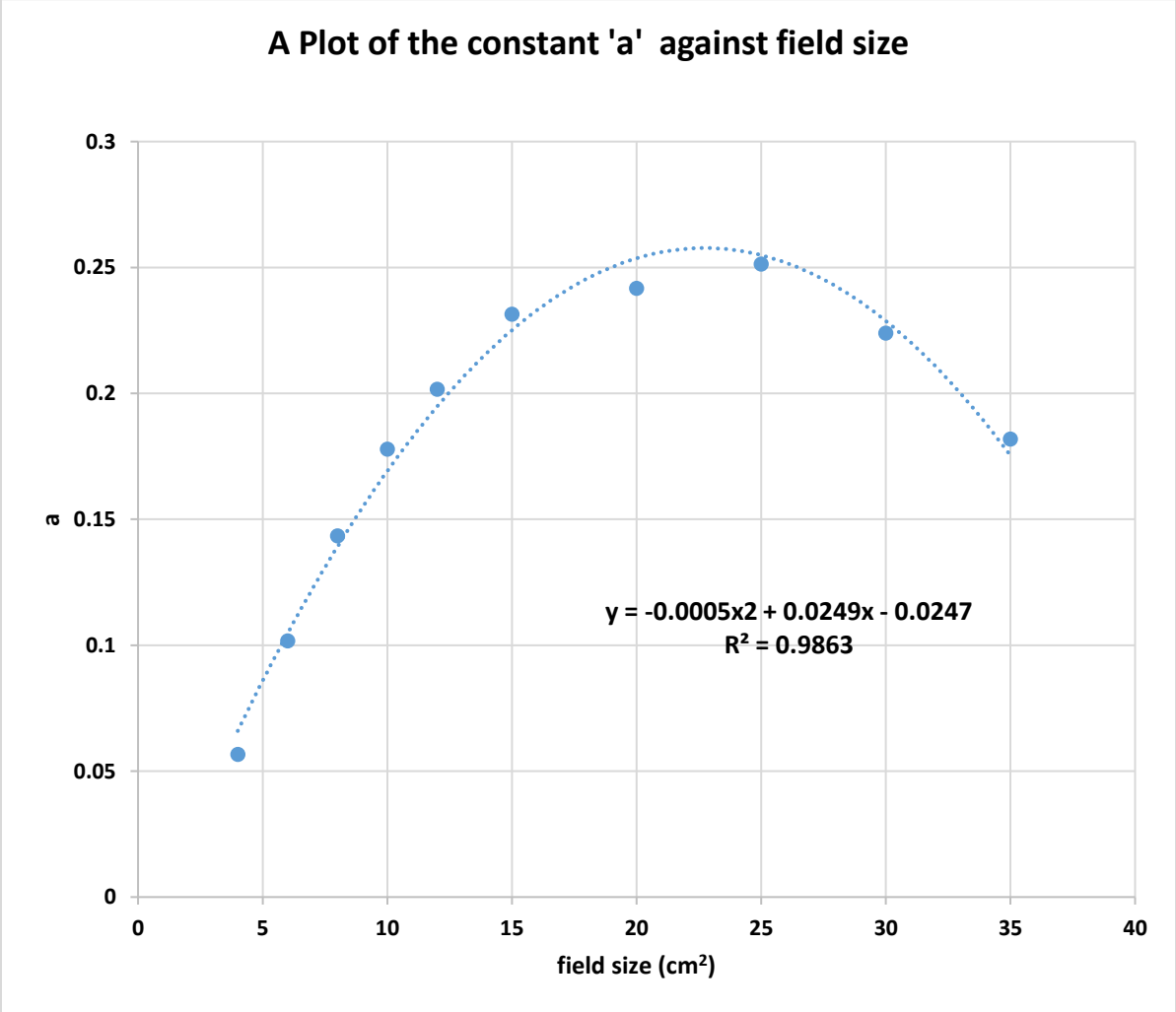

Appendix W: Figure 9

A Plot of the constant 'b' against field size